

Geometry and material effects in Casimir physics - Scattering theory

Sahand Jamal Rahi, Thorsten Emig, and Robert L. Jaffe

Abstract We give a comprehensive presentation of methods for calculating the Casimir force to arbitrary accuracy, for any number of objects, arbitrary shapes, susceptibility functions, and separations. The technique is applicable to objects immersed in media other than vacuum, to nonzero temperatures, and to spatial arrangements in which one object is enclosed in another. Our method combines each object's classical electromagnetic scattering amplitude with universal translation matrices, which convert between the bases used to calculate scattering for each object, but are otherwise independent of the details of the individual objects. This approach, which combines methods of statistical physics and scattering theory, is well suited to analyze many diverse phenomena. We illustrate its power and versatility by a number of examples, which show how the interplay of geometry and material properties helps to understand and control Casimir forces. We also examine whether electrodynamic Casimir forces can lead to stable levitation. Neglecting permeabilities, we prove that any equilibrium position of objects subject to such forces is unstable if the permittivities of all objects are higher or lower than that of the enveloping medium; the former being the generic case for ordinary materials in vacuum.

S. J. Rahi

Department of Physics, MIT, Cambridge, MA, e-mail: sjrahi@mit.edu

T. Emig

Institut für Theoretische Physik, Universität zu Köln, Zùlpicher Strasse 77, 50937 Köln, Germany and Laboratoire de Physique Théorique et Modèles Statistiques, CNRS UMR 8626, Université Paris-Sud, 91405 Orsay, France, e-mail: emig@lptms.u-psud.fr

R. L. Jaffe

Center for Theoretical Physics MIT, Cambridge, MA, e-mail: jaffe@mit.edu

1 Introduction

Neutral objects exert a force on one another through electromagnetic fields even if they do not possess permanent multipole moments. Materials that couple to the electromagnetic field alter the spectrum of the field's quantum and thermal fluctuations. The resulting change in energy depends on the relative positions of the objects, leading to a fluctuation-induced force, usually called the Casimir force. Alternatively, one can regard the cause of these forces to be spontaneous charges and currents, which fluctuate in and out of existence in the objects due to quantum mechanics. The name 'Van der Waals force' is sometimes used interchangeably but it usually refers to the Casimir force in the regime where objects are close enough to one another that the speed of light is effectively infinite. The Casimir force has been the subject of precision experimental measurements [59, 69, 88, 27, 16, 20, 24, 46, 18, 55, 23, 19, 71, 17, 53, 73, 72] and can influence the operation of nanoscale devices [16, 13], see reference [54] for a review of the experiments.

Casimir and Polder calculated the fluctuation-induced force on a polarizable atom in front of a perfectly conducting plate and between two polarizable atoms, both to leading order at large separation, and obtained a simple result depending only on the atoms' static polarizabilities [15]. Casimir then extended this result to his famous calculation of the pressure on two perfectly conducting parallel plates [14]. Feinberg and Sucher [34, 35] generalized the result of Casimir and Polder to include both electric and magnetic polarizabilities. Lifshitz, Dzyaloshinskii, and Pitaevskii extended Casimir's result for parallel plates by incorporating nonzero temperature, permittivity, and permeability into a general formula for the pressure on two infinite half-spaces separated by a gap [64, 25, 65].

While these early theoretical predictions of the Casimir force applied only to infinite planar geometries (or atoms), the first precision experiments measured the force between a plate and a sphere. This geometry was preferred because keeping two plane surfaces parallel introduces additional challenges for the experimentalist. To compare the measurements with theory, however, a makeshift solution had to be used: known as the Proximity Force Approximation (PFA), it estimates the Casimir force by integrating the Casimir pressure between opposing infinitesimal surface area elements, as if they were parallel plates, over the area that the sphere and the plate expose to one another [74]. In general, this simple approximation does not capture curvature corrections but in many experimental situations, it performs surprisingly well, as can be seen in Fig. 1, for example; at the small separations at which the force is typically probed in precision measurements the sphere and the plate surfaces are well approximated by a collection of infinitesimal parallel plates.

Clearly, for larger separations and for surfaces that are not smooth, the PFA must fail. For example, in measurements of the Casimir force between a sphere and a trench array significant discrepancies were found [17]. And even for the regimes in which the PFA yields good estimates it would be desirable to know what the corrections are.

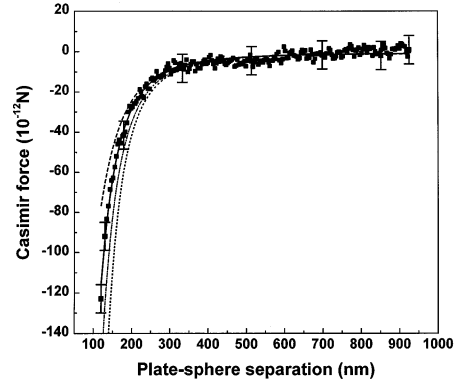


Fig. 1 Force between a sphere of radius $\approx 100\mu\text{m}$ and a plate, both coated with Au-Pd [69]. Square dots represent measurements, the solid line is a theoretical computation using the PFA approximation and taking into account roughness and finite temperature corrections as well as material properties. The other lines represent calculations, where some of these corrections are not taken into account.

In order to study Casimir forces in more general geometries, it turns out to be advantageous to describe the influence of an arrangement of objects on the electromagnetic field by the way they scatter electromagnetic waves. Here, we derive and apply a representation of the Casimir energy, first developed with various limitations in Refs. [28, 29] and then fully generalized in Ref. [75], that characterizes each object by its on-shell electromagnetic scattering amplitude. The separations and orientations of the objects are encoded in universal translation matrices, which describe how a solution to the source-free Maxwell's equations in the basis appropriate to one object looks when expanded in the basis appropriate to another. The translation matrices depend on the displacement and orientation of coordinate systems, but not on the nature of the objects themselves. The scattering amplitudes and translation matrices are then combined in a simple algorithm that allows efficient numerical and, in some cases, analytical calculations of Casimir forces and torques for a wide variety of geometries, materials, and external conditions. The formalism applies to a wide variety of circumstances, including:

- n arbitrarily shaped objects, whose surfaces may be smooth or rough or may include edges and cusps;
- objects with arbitrary linear electromagnetic response, including frequency-dependent, lossy electric permittivity and magnetic permeability tensors;
- objects separated by vacuum or by a medium with uniform, frequency-dependent isotropic permittivity and permeability;
- zero or nonzero temperature;
- and objects outside of one another or enclosed in each other.

These ideas build on a range of previous related work, an inevitably incomplete subset of which is briefly reviewed here: Scattering theory methods were first ap-

plied to the parallel plate geometry, when Kats reformulated Lifshitz theory in terms of reflection coefficients [50]. Jaekel and Reynaud derived the Lifshitz formula using reflection coefficients for lossless infinite plates [48] and Genet, Lambrecht, and Reynaud extended this analysis to the lossy case [38]. Lambrecht, Maia Neto, and Reynaud generalized these results to include non-specular reflection [58].

Around the same time as Kats's work, Balian and Duplantier developed a multiple scattering approach to the Casimir energy for perfect metal objects and used it to compute the Casimir energy at asymptotically large separations [4, 5] at both zero and nonzero temperature. In their approach, information about the conductors is encoded in a local surface scattering kernel, whose relation to more conventional scattering formalisms is not transparent, and their approach was not pursued further at the time. One can find multiple scattering formulas in an even earlier article by Renne [81], but scattering is not explicitly mentioned, and the technique is only used to rederive older results.

Another scattering-based approach has been to express the Casimir energy as an integral over the density of states of the fluctuating field, using the Krein formula [56, 57, 6] to relate the density of states to the S -matrix for scattering from the ensemble of objects. This S -matrix is difficult to compute in general. In studying many-body scattering, Henseler and Wirzba connected the S -matrix of a collection of spheres [47] or disks [93] to the objects' individual S -matrices, which are easy to find. Bulgac, Magierski, and Wirzba combined this result with the Krein formula to investigate the scalar and fermionic Casimir effect for disks and spheres [11, 10, 94]. Casimir energies of solitons in renormalizable quantum field theories have been computed using scattering theory techniques that combine analytic and numerical methods [44].

Bordag, Robaschik, Scharnhorst, and Wieczorek [7, 82] introduced path integral methods to the study of Casimir effects and used them to investigate the electromagnetic Casimir effect for two parallel perfect metal plates. Li and Kardar used similar methods to study the scalar thermal Casimir effect for Dirichlet, Neumann, and mixed boundary conditions [62, 63]. The quantum extension was developed further by Golestanian and Kardar [41, 42] and was subsequently applied to the quantum electromagnetic Casimir effect by Emig, Hanke, Golestanian, and Kardar, who studied the Casimir interaction between plates with roughness [31] and between deformed plates [32]. (Techniques developed to study the scalar Casimir effect can be applied to the electromagnetic case for perfect metals with translation symmetry in one spatial direction, since then the electromagnetic problem decomposes into two scalar ones.) Finally, the path integral approach was connected to scattering theory by Emig and Buescher [12].

Closely related to the work we present here is that of Kenneth and Klich, who expressed the data required to characterize Casimir fluctuations in terms of the transition \mathbb{T} -operator for scattering of the fluctuating field from the objects [51]. Their abstract representation made it possible to prove general properties of the sign of the Casimir force. In Refs. [28, 29], we developed a framework in which this abstract result can be applied to concrete calculations. In this approach, the \mathbb{T} -operator is related to the scattering amplitude for each object individually, which in turn is

expressed in an appropriate basis of multipoles. While the \mathbb{T} -operator is in general “off-shell,” meaning it has matrix elements between states with different spatial frequencies, the scattering amplitudes are the “on-shell” matrix elements of this operator between states of equal spatial frequency.¹ So, it is not the \mathbb{T} -operator itself that connects, say, outgoing and standing waves in the case of outside scattering but its on-shell matrix elements, the scattering amplitudes. In this approach, the objects can have any shape or material properties, as long as the scattering amplitude can be computed in a multipole expansion (or measured). The approach can be regarded as a concrete implementation of the proposal emphasized by Schwinger [90] that the fluctuations of the electromagnetic field can be traced back to charge and current fluctuations on the objects. This formalism has been applied and extended in a number of Casimir calculations [52, 67, 68, 80, 40, 91].

The basis in which the scattering amplitude for each object is supplied is typically associated with a coordinate system appropriate to the object. Of course a plane, a cylinder, or a sphere would be described in Cartesian, cylindrical, or spherical coordinates, respectively. However, any compact object can be described, for example, in spherical coordinates, provided that the matrix of scattering amplitudes can be either calculated or measured in that coordinate system. There are a limited number of coordinate systems in which such a partial wave expansion is possible, namely those for which the vector Helmholtz equation is separable. The translation matrices for common separable coordinate systems, obtained from the free Green’s function, are supplied in Appendix C of reference [75]. For typical cases, the final computation of the Casimir energy can be performed on a desktop computer for a wide range of separations. Asymptotic results at large separation can be obtained analytically.

The primary limitation of the method is on the distance between objects, since the basis appropriate to a given object may become impractical as two objects approach. For small separations, sufficient accuracy can only be obtained if the calculation is taken to very high partial wave order. (Vastly different scales are problematic for numerical evaluations in general.) In the case of two spheres, the scattering amplitude is available in a spherical basis, but as the two spheres approach, the Casimir energy is dominated by waves near the point of closest approach [89]. As the spheres come into contact an infinite number of spherical waves are needed to capture the dominant contribution. A particular basis may also be fundamentally inappropriate at small separations. For instance, if the interaction of two elliptic cylinders is expressed in an ordinary cylindrical basis, when the elliptic cylinders are close enough, the smallest circular cylinder enclosing one may not lie outside the smallest circular cylinder enclosing the other. In that case the cylindrical basis would not “resolve” the two objects (although an elliptic cylindrical basis would). Finally, for a variety of conceptual and computational reasons, we are limited to linear electromagnetic response.

¹ Because of this relationship, these scattering amplitudes are also referred to as elements of the *T*-matrix. In standard conventions, however, the *T*-matrix differs from the matrix elements of the \mathbb{T} -operator by a basis-dependent constant, so we will use the term “scattering amplitude” to avoid confusion.

In spirit and in mathematical form our final result resembles similar expressions obtained in surface integral equation methods used in computational electrodynamics [21]. Using such a formulation, in which the unknowns are currents and fields on the objects, one can compute the Casimir energy using more general basis functions, e.g., localized basis functions associated with a grid or mesh, giving rise to finite element and boundary elements methods [80].

In addition to an efficient computational approach, the scattering formalism has provided the basis for proving general theorems regarding Casimir forces. The seemingly natural question whether the force is attractive or repulsive turns out to be an ill-defined or, at least, a tricky one on closer inspection. When, for example, many bodies are considered, the direction of the force on any one object depends, of course, on which other object’s perspective one takes. Even for two objects, “attractive” forces can be arranged to appear as a “repulsive” force, as in the case of two interlocking combs [84]. To avoid such ambiguous situations one can restrict oneself to analyzing two objects that are separable by a plane. Even here, it has turned out that a simple criterion for the direction of the force could not be found. Based on various calculations for simple geometries it was thought that the direction of the force can be predicted based on the relative permittivities and permeabilities of the objects and the medium. Separating materials into two groups, with (i) permittivity higher than the medium or permeability lower than the medium ($\epsilon > \epsilon_M$ and $\mu \leq \mu_M$), or (ii) the other way around ($\epsilon < \epsilon_M$ and $\mu \geq \mu_M$), Casimir forces had been found to be attractive between members of the same group and repulsive for different types in the geometries considered. However, a recent counterexample [61] shows that this is not always true. A rigorous theorem, which states that Casimir forces are always attractive, exists only for the special case of mirror symmetric arrangements of objects. It was proven first with a \mathbb{T} -operator formalism [51], similar to our approach used here, and later using reflection positivity [3]. We have taken an alternative characterization of the force to be fundamental, namely, whether it can produce a stable equilibrium [77]. Here, the categorization of materials into the two groups is meaningful since objects made of materials of the same type cannot produce stable levitation. One practical consequence of this theorem is that it reveals that many current proposals for producing levitation using metamaterials cannot succeed.

To illustrate the general formulation, we provide some sample applications. We include an analysis of the forces between two cylinders or wires [76] and a cylinder and a plate [33, 76, 75]. The Casimir interaction of three bodies is presented subsequently; it reveals interesting multibody effects [78, 76, 85]. The Casimir torque of two spheroids is discussed as well [30]. Furthermore, we analyze the Casimir effect for a parabolic cylinder opposite a plate when both represent perfect metal material boundary conditions [45]. We find that the Casimir force does not vanish in the limit of an infinitesimally thin parabola, where a half plate is arranged above an infinite plate, and we compute the edge effect. Another type of geometries that is treated here consists of a finite sphere or a small spheroid inside a spherical metallic cavity [95].

This chapter is organized as follows: First, we sketch the derivation of the Casimir interaction energy formula Eq. (39) in Section 2. Next, the theorem re-

garding stability is derived in Section 3. Finally, in Section 4 sample applications are presented.

2 General theory for Casimir interactions

This section has been adapted from a longer article, reference [75]. Many technical details and extensive appendices have been omitted to fit the format of this book.

2.1 Path integral quantization

2.1.1 Electromagnetic Lagrangian

We consider the Casimir effect for objects without free charges and currents but with nonzero electric and magnetic susceptibilities. The macroscopic electromagnetic Lagrangian density is

$$\mathcal{L} = \frac{1}{2}(\mathbf{E} \cdot \mathbf{D} - \mathbf{B} \cdot \mathbf{H}). \quad (1)$$

The electric field $\mathbf{E}(t, \mathbf{x})$ and the magnetic field $\mathbf{B}(t, \mathbf{x})$ are related to the fundamental four-vector potential A^μ by $\mathbf{E} = -c^{-1} \partial_t \mathbf{A} - \nabla A^0$ and $\mathbf{B} = \nabla \times \mathbf{A}$. We treat stationary objects whose responses to the electric and magnetic fields are linear. For such materials, the \mathbf{D} and \mathbf{B} fields are related to the \mathbf{E} and \mathbf{H} fields by the convolutions $\mathbf{D}(t, \mathbf{x}) = \int_{-\infty}^{\infty} dt' \varepsilon(t', \mathbf{x}) \mathbf{E}(t - t', \mathbf{x})$ and $\mathbf{B}(t, \mathbf{x}) = \int_{-\infty}^{\infty} dt' \mu(t', \mathbf{x}) \mathbf{H}(t - t', \mathbf{x})$ in time, where $\varepsilon(t', \mathbf{x})$ and $\mu(t', \mathbf{x})$ vanish for $t' < 0$. We consider local, isotropic permittivity and permeability, although our derivation can be adapted to apply to non-local and non-isotropic media simply by substituting the appropriate non-local and tensor permittivity and permeability functions. A more formal derivation of our starting point Eq. (1), which elucidates the causality properties of the permeability and permittivity response functions, is given in Appendix A of reference [75].

We define the quantum-mechanical energy through the path integral, which sums all configurations of the electromagnetic fields constrained by periodic boundary conditions in time between 0 and T . Outside of this time interval the fields are periodically continued. Substituting the Fourier expansions of the form $\mathbf{E}(t, \mathbf{x}) = \sum_{n=-\infty}^{\infty} \mathbf{E}(\omega_n, \mathbf{x}) e^{-i\omega_n t}$ with $\omega_n = 2\pi n/T$, we obtain the action

$$S(T) = \frac{1}{2} \int_0^T dt \int d\mathbf{x} (\mathbf{E} \cdot \mathbf{D} - \mathbf{B} \cdot \mathbf{H}) = \frac{1}{2} T \sum_{n=-\infty}^{\infty} \int d\mathbf{x} (\mathbf{E}^* \cdot \varepsilon \mathbf{E} - \mathbf{B}^* \cdot \mu^{-1} \mathbf{B}), \quad (2)$$

where ε , \mathbf{E} , μ , and \mathbf{B} on the right-hand side are functions of position \mathbf{x} and frequency ω_n , and we have used $\mathbf{D}(\omega, \mathbf{x}) = \varepsilon(\omega, \mathbf{x}) \mathbf{E}(\omega, \mathbf{x})$ and $\mathbf{H}(\omega, \mathbf{x}) = \frac{1}{\mu(\omega, \mathbf{x})} \mathbf{B}(\omega, \mathbf{x})$.

From the definition of the fields \mathbf{E} and \mathbf{B} in terms of the vector potential A^μ , we have $\nabla \times \mathbf{E} = i\frac{\omega}{c}\mathbf{B}$, which enables us to eliminate \mathbf{B} in the action,

$$S(T) = \frac{1}{2}T \sum_{n=-\infty}^{\infty} \int d\mathbf{x} \left[\mathbf{E}^* \cdot \left(\mathbb{I} - \frac{c^2}{\omega_n^2} \nabla \times \nabla \times \right) \mathbf{E} - \frac{c^2}{\omega_n^2} \mathbf{E}^* \cdot \nabla \mathbf{E} \right], \quad (3)$$

where

$$\mathbb{V} = \mathbb{I} \frac{\omega_n^2}{c^2} (1 - \varepsilon(\omega_n, \mathbf{x})) + \nabla \times \left(\frac{1}{\mu(\omega_n, \mathbf{x})} - 1 \right) \nabla \times \quad (4)$$

is the potential operator and we have restored the explicit frequency dependence of ε and μ . The potential operator is nonzero only at those points in space where the objects are located ($\varepsilon \neq 1$ or $\mu \neq 1$).

In the functional integral we will sum over configurations of the field A^μ . This sum must be restricted by a choice of gauge, so that it does not include the infinitely redundant gauge orbits. We choose to work in the gauge $A^0 = 0$, although of course no physical results depend on this choice.

2.1.2 Casimir energy from Euclidean action

We use standard tools to obtain a functional integral expression for the ground state energy of a quantum field in a fixed background described by $\mathbb{V}(\omega, \mathbf{x})$. The overlap between the initial state $|\mathbf{E}_a\rangle$ of a system with the state $|\mathbf{E}_b\rangle$ after time T can be expressed as a functional integral with the fields fixed at the temporal boundaries [36],

$$\langle \mathbf{E}_b | e^{-iHT/\hbar} | \mathbf{E}_a \rangle = \int \mathcal{D}\mathbf{A} \Big|_{\substack{\mathbf{E}(t=0)=\mathbf{E}_a \\ \mathbf{E}(t=T)=\mathbf{E}_b}} e^{\frac{i}{\hbar}S(T)}, \quad (5)$$

where $S(T)$ is the action of Eq. (2) with the time integrals taken between zero and T , and H is the corresponding Hamiltonian.

If the initial and final states are set equal and summed over, the resulting functional integration defines the Minkowski space functional integral

$$\mathcal{Z}(T) \equiv \sum_a \langle \mathbf{E}_a | e^{-iHT/\hbar} | \mathbf{E}_a \rangle = \text{tr} e^{-iHT/\hbar} = \int \mathcal{D}\mathbf{A} e^{\frac{i}{\hbar}S(T)}, \quad (6)$$

which depends on the time T and the background potential $\mathbb{V}(\omega, \mathbf{x})$. The partition function that describes this system at temperature $1/\beta$ is defined by

$$Z(\beta) = \mathcal{Z}(-i\hbar\beta) = \text{tr} e^{-\beta H}, \quad (7)$$

and the free energy F of the field is

$$F(\beta) = -\frac{1}{\beta} \log Z(\beta). \quad (8)$$

The limit $\beta \rightarrow \infty$ projects the ground state energy out of the trace,

$$\mathcal{E}_0 = F(\beta = \infty) = - \lim_{\beta \rightarrow \infty} \frac{1}{\beta} \log Z(\beta). \quad (9)$$

The unrenormalized energy \mathcal{E}_0 generally depends on an ultraviolet cutoff, but cutoff-dependent contributions arise from the objects individually [43, 44] and do not depend on their separations or orientations. Such terms can remain after ordinary QED renormalization if objects are assumed to constrain electromagnetic waves with arbitrarily high frequencies (for example, if the fields are forced to vanish on a surface). Such boundary conditions should be regarded as artificial idealizations; in reality, when the wavelengths of the electromagnetic waves become shorter than the length scales that characterize the interactions of the material, the influence of the material on the waves vanishes [43]. Accordingly, the potential \mathbb{V} should vanish for real materials in the high-frequency limit. In any event these cutoff dependences are independent of the separation and orientation of the objects, and since we are only interested in energy *differences*, we can remove them by subtracting the ground state energy of the system when the objects are in some reference configuration. In most cases we take this configuration to be when the objects are infinitely far apart, but when calculating Casimir energies for one object inside another, some other configuration must be used. We denote the partition function for this reference configuration by \bar{Z} . In this way we obtain the Casimir energy,

$$\mathcal{E} = - \lim_{\beta \rightarrow \infty} \frac{1}{\beta} \log Z(\beta) / \bar{Z}(\beta). \quad (10)$$

Throughout our calculation of \mathcal{E} , we will thus be able to neglect any overall factors that are independent of the relative positions and orientations of the objects.

By replacing the time T by $-i\hbar\beta$, we transform the Minkowski space functional integral $\mathcal{Z}(T)$ into the partition function $Z(\beta)$. In $A^0 = 0$ gauge, the result is simply to replace the frequencies $\omega_n = \frac{2\pi n}{T}$ in Eq. (4) by $i\frac{2\pi n}{\hbar\beta} = ic\kappa_n$, where κ_n is the n^{th} Matsubara frequency divided by c . (In other gauges the temporal component A^0 of the vector field must be rotated too.)

The Lagrangian is quadratic, so the modes with different κ_n decouple and the partition function decomposes into a product of partition functions for each mode. Since the electromagnetic field is real, we have $\mathbf{E}^*(\omega) = \mathbf{E}(-\omega)$ on the real axis. We can thus further simplify this decomposition on the imaginary axis by considering $\kappa \geq 0$ only, but allowing \mathbf{E} and \mathbf{E}^* to vary independently in the path integral. Restricting to positive κ is possible because the response functions $\epsilon(ic\kappa, \mathbf{x})$ and $\mu(ic\kappa, \mathbf{x})$ are invariant under a change of sign in $ic\kappa$, as shown in Appendix A of Ref. [75]. In the limit $\beta \rightarrow \infty$, the sum $\sum_{n \geq 0}$ turns into an integral $\frac{\hbar c \beta}{2\pi} \int_0^\infty d\kappa$, and we have

$$\mathcal{E}_0 = - \frac{\hbar c}{2\pi} \int_0^\infty d\kappa \log Z(\kappa), \quad (11)$$

where

$$Z(\kappa) = \int \mathcal{D}\mathbf{A} \mathcal{D}\mathbf{A}^* \exp \left[-\beta \int d\mathbf{x} \mathbf{E}^* \cdot \left(\mathbb{I} + \frac{1}{\kappa^2} \nabla \times \nabla \times \right) \mathbf{E} + \frac{1}{\kappa^2} \mathbf{E}^* \cdot \nabla (i\kappa \mathbf{x}) \mathbf{E} \right], \quad (12)$$

$$\nabla (i\kappa \mathbf{x}) = \mathbb{I} \kappa^2 (\varepsilon(i\kappa \mathbf{x}) - 1) + \nabla \times \left(\frac{1}{\mu(i\kappa \mathbf{x})} - 1 \right) \nabla \times. \quad (13)$$

The potential $\nabla (i\kappa \mathbf{x})$ is real for real κ , even though ε and μ can have imaginary parts for real frequencies ω . Our goal is now to manipulate $Z(\kappa)$ in Eq. (12) so that it is computable from the scattering properties of the objects.

2.2 Green's function expansions and translation formulas

The free Green's function and its representations in various coordinate systems are crucial to our formalism. The free electromagnetic field ($\mathbb{V} = 0$) obeys equations of motion obtained by extremizing the corresponding action, Eq. (2),

$$\left(-\mathbb{I} \frac{\omega^2}{c^2} + \nabla \times \nabla \times \right) \mathbf{E}(\omega, \mathbf{x}) = 0. \quad (14)$$

We will employ the electromagnetic dyadic Green's function \mathbb{G}_0 , defined by

$$\left(-\mathbb{I} \frac{\omega^2}{c^2} + \nabla \times \nabla \times \right) \mathbb{G}_0(\omega, \mathbf{x}, \mathbf{x}') = \mathbb{I} \delta^{(3)}(\mathbf{x} - \mathbf{x}'), \quad (15)$$

written here in the position space representation. The Green's function has to be the retarded one, not only on physical grounds, but also as a consequence of the imaginary-frequency formalism, just as is the case for the response functions ε and μ . It is the *retarded* response functions that are analytically continued in the frequency domain to positive imaginary frequency, as shown in Appendix A of reference [75].

The representation of the free Green's function, which we need, employs the “regular” and “outgoing” solutions to the differential equation, Eq. (14),

$$\mathbf{E}_\alpha^{\text{reg}}(\omega, \mathbf{x}) = \langle \mathbf{x} | \mathbf{E}_\alpha^{\text{reg}}(\omega) \rangle, \quad \mathbf{E}_\alpha^{\text{out}}(\omega, \mathbf{x}) = \langle \mathbf{x} | \mathbf{E}_\alpha^{\text{out}}(\omega) \rangle, \quad (16)$$

represented formally by the eigenstate kets $|\mathbf{E}_\alpha^{\text{reg}}(\omega)\rangle$ and $|\mathbf{E}_\alpha^{\text{out}}(\omega)\rangle$, where the generalized index α labels the scattering channel, including the polarization. For example, for spherical wave functions it represents the angular momentum quantum numbers (l, m) and the polarization E or M . There are six coordinate systems in which the vector wave equation (14) can be solved by separation of variables and vector wave functions appropriate to that coordinate system can be constructed [70]. The labels “regular” and “outgoing” denote, respectively, the wave functions' non-singular behavior at the origin or ‘outward’ direction of energy transport along one of the coordinate system's axes. Let us call the coordinate, along which the latter

wave functions are outgoing ξ_1 and the other coordinates ξ_2 and ξ_3 . We will usually work on the imaginary ω -axis, in which case we will encounter the corresponding modified special functions.

The free Green's function can be expanded in tensor products of these wave functions,

$$\mathbb{G}_0(\omega, \mathbf{x}, \mathbf{x}') = \sum_{\alpha} C_{\alpha}(\omega) \begin{cases} \mathbf{E}_{\alpha}^{\text{out}}(\omega, \xi_1, \xi_2, \xi_3) \otimes \mathbf{E}_{\alpha}^{\text{reg}*}(\omega, \xi'_1, \xi'_2, \xi'_3) & \text{if } \xi_1(\mathbf{x}) > \xi'_1(\mathbf{x}') \\ \mathbf{E}_{\alpha}^{\text{reg}}(\omega, \xi_1, \xi_2, \xi_3) \otimes \mathbf{E}_{\alpha}^{\text{in}*}(\omega, \xi'_1, \xi'_2, \xi'_3) & \text{if } \xi_1(\mathbf{x}) < \xi'_1(\mathbf{x}') \end{cases}, \quad (17)$$

$\mathbf{E}_{\alpha}^{\text{in}}$ is the same as $\mathbf{E}_{\alpha}^{\text{out}}$ except the functional dependence on ξ_1 is complex conjugated, making the wave function ‘incoming’. A list of Green's function expansions in various common bases, including the normalization constant, $C_{\alpha}(\omega)$, is given in Appendix B of Ref. [75]. The wave functions that appear in the series expansion of the free Green's functions in Eq. (17) satisfy wave equations with frequency ω . As we will see in Sec. 2.3, the ability to express the Casimir energy entirely in terms of an ‘on-shell’ partial wave expansion with fixed ω will greatly simplify our calculations.

We will also use the free Green's function in another representation to combine the scattering amplitudes for two different objects. In this calculation the one argument of the Green's function will be located on each object. As long as the pair of objects can be separated in one of the separable coordinate systems by the surface $\xi_1 = \bar{\varepsilon} = \text{const.}$, we can distinguish an inside object which lies entirely inside the surface ($\xi_1 < \bar{\varepsilon}$) and an outside object ($\xi_1 > \bar{\varepsilon}$), see Fig. 2. Then, we can expand

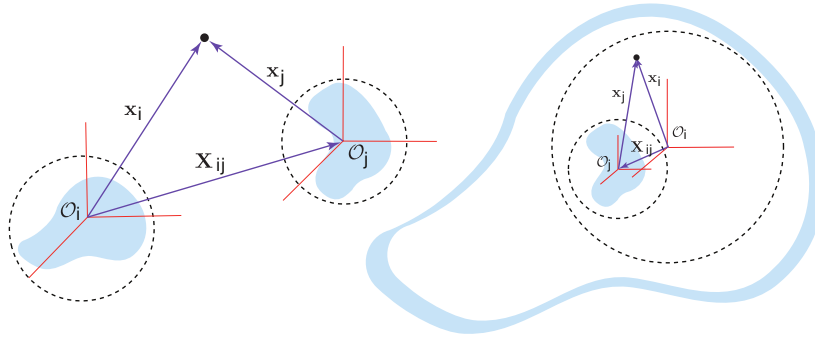


Fig. 2 Geometry of the outside (left) and inside (right) configurations. The dotted lines show surfaces separating the objects on which the radial variable is constant. The translation vector $\mathbf{X}_{ij} = \mathbf{x}_i - \mathbf{x}_j = -\mathbf{X}_{ji}$ describes the relative positions of the two origins.

the free Green's function, when one argument, say \mathbf{x} , lies on object i and the other argument, say \mathbf{x}' , lies on object j , we expand $\mathbb{G}_0(ic\boldsymbol{\kappa}, \mathbf{x}, \mathbf{x}')$ in terms of coordinates \mathbf{x}_i and \mathbf{x}'_j that describe each point relative to the origin of the body on which it lies. Which of the following expansions is appropriate for a particular pair of objects depends whether objects i and j are outside of one another, or one object is inside the other,

$$\mathbb{G}_0(ic\boldsymbol{\kappa}, \mathbf{x}, \mathbf{x}') = \sum_{\alpha, \beta} C_\beta(\boldsymbol{\kappa}) \begin{cases} \mathbf{E}_\alpha^{\text{reg}}(\boldsymbol{\kappa}, \mathbf{x}_i) \otimes \mathcal{W}_{\alpha\beta}^{ji}(\boldsymbol{\kappa}) \mathbf{E}_\beta^{\text{reg}*}(\boldsymbol{\kappa}, \mathbf{x}'_j) & \text{if } i \text{ and } j \text{ are outside each other} \\ \mathbf{E}_\alpha^{\text{reg}}(\boldsymbol{\kappa}, \mathbf{x}_i) \otimes \mathcal{V}_{\alpha\beta}^{ij}(\boldsymbol{\kappa}) \mathbf{E}_\beta^{\text{in}*}(\boldsymbol{\kappa}, \mathbf{x}'_j) & \left\{ \begin{array}{l} \text{if } i \text{ is inside } j, \text{ or} \\ \text{if } i \text{ is below } j \text{ (plane wave basis)} \end{array} \right. \\ \mathbf{E}_\alpha^{\text{out}}(\boldsymbol{\kappa}, \mathbf{x}_i) \otimes \mathcal{W}_{\alpha\beta}^{ji}(\boldsymbol{\kappa}) \mathbf{E}_\beta^{\text{reg}*}(\boldsymbol{\kappa}, \mathbf{x}'_j) & \left\{ \begin{array}{l} \text{if } j \text{ is inside } i, \text{ or} \\ \text{if } j \text{ is below } i \text{ (plane wave basis)} \end{array} \right. \end{cases} \quad (18)$$

where $\mathcal{W}_{\alpha\beta}^{ji}(\boldsymbol{\kappa}) = \mathcal{V}_{\alpha\beta}^{ji, \dagger}(\boldsymbol{\kappa}) \frac{C_\alpha(\boldsymbol{\kappa})}{C_\beta(\boldsymbol{\kappa})}$ and C_α is the normalization constant defined in Eq. (17). The expansion can be written more compactly as

$$\mathbb{G}_0(ic\boldsymbol{\kappa}) = \sum_{\alpha, \beta} (-C_\beta(\boldsymbol{\kappa})) (|\mathbf{E}_\alpha^{\text{reg}}(\boldsymbol{\kappa})\rangle \langle \mathbf{E}_\alpha^{\text{out}}(\boldsymbol{\kappa})|) \mathbb{X}_{\alpha\beta}^{ij}(\boldsymbol{\kappa}) \begin{pmatrix} \langle \mathbf{E}_\beta^{\text{reg}}(\boldsymbol{\kappa}) | \\ \langle \mathbf{E}_\beta^{\text{in}}(\boldsymbol{\kappa}) | \end{pmatrix}, \quad (19)$$

where the \mathbb{X} matrix is defined, for convenience, as the negative of the matrix containing the translation matrices,

$$\mathbb{X}^{ij}(\boldsymbol{\kappa}) = \begin{pmatrix} -\mathcal{W}^{ji}(\boldsymbol{\kappa}) & -\mathcal{V}^{ij}(\boldsymbol{\kappa}) \\ -\mathcal{W}^{ji}(\boldsymbol{\kappa}) & 0 \end{pmatrix}. \quad (20)$$

In Eq. (19) the bras and kets are to be evaluated in position space in the appropriately restricted domains and only one of the three submatrices is nonzero for any pair of objects i and j as given in Eq. (18). The translation matrices for various geometries are provided in Appendix C of reference [75].

2.3 Classical scattering of electromagnetic fields

In this section, we summarize the key results from scattering theory needed to compute the scattering amplitude of each body individually. In the subsequent section we will then combine these results with the translation matrices of the previous section to compute $Z(\boldsymbol{\kappa})$.

By combining the frequency-dependent Maxwell equations, one obtains the vector wave equation

$$(\mathbb{H}_0 + \mathbb{V}(\boldsymbol{\omega}, \mathbf{x}))\mathbf{E}(\boldsymbol{\omega}, \mathbf{x}) = \frac{\boldsymbol{\omega}^2}{c^2} \mathbf{E}(\boldsymbol{\omega}, \mathbf{x}), \quad (21)$$

where

$$\begin{aligned} \mathbb{H}_0 &= \nabla \times \nabla \times, \\ \mathbb{V}(\omega, \mathbf{x}) &= \mathbb{I} \frac{\omega^2}{c^2} (1 - \varepsilon(\omega, \mathbf{x})) + \nabla \times \left(\frac{1}{\mu(\omega, \mathbf{x})} - 1 \right) \nabla \times, \end{aligned} \quad (22)$$

which is the same potential operator as the one obtained by rearranging the Lagrangian (see Eq. (4)).

The Lippmann-Schwinger equation [66]

$$|\mathbf{E}\rangle = |\mathbf{E}_0\rangle - \mathbb{G}_0 \mathbb{V} |\mathbf{E}\rangle \quad (23)$$

expresses the general solution to Eq. (21). Here, \mathbb{G}_0 is the free electromagnetic tensor Green's function discussed in Sec. 2.2 and the homogeneous solution $|\mathbf{E}_0\rangle$ obeys $\left(-\frac{\omega^2}{c^2} \mathbb{I} + \mathbb{H}_0\right) |\mathbf{E}_0\rangle = 0$. We can iteratively substitute for $|\mathbf{E}\rangle$ in Eq. (23) to obtain the formal expansion

$$\begin{aligned} |\mathbf{E}\rangle &= |\mathbf{E}_0\rangle - \mathbb{G}_0 \mathbb{V} |\mathbf{E}_0\rangle + \mathbb{G}_0 \mathbb{V} \mathbb{G}_0 \mathbb{V} |\mathbf{E}_0\rangle - \dots \\ &= |\mathbf{E}_0\rangle - \mathbb{G}_0 \mathbb{T} |\mathbf{E}_0\rangle, \end{aligned} \quad (24)$$

where the electromagnetic \mathbb{T} -operator is defined as

$$\mathbb{T} = \mathbb{V} \frac{\mathbb{I}}{\mathbb{I} + \mathbb{G}_0 \mathbb{V}} = \mathbb{V} \mathbb{G} \mathbb{G}_0^{-1}, \quad (25)$$

and \mathbb{G} is the Green's function of the full Hamiltonian, $\left(-\frac{\omega^2}{c^2} \mathbb{I} + \mathbb{H}_0 + \mathbb{V}\right) \mathbb{G} = \mathbb{I}$. We note that \mathbb{T} , \mathbb{G}_0 , and \mathbb{G} are all functions of frequency ω and non-local in space. As can be seen from expanding \mathbb{T} in Eq. (25) in a power series, $\langle \mathbf{x} | \mathbb{T}(\omega) | \mathbf{x}' \rangle$ is zero whenever \mathbf{x} or \mathbf{x}' are not located on an object, *i.e.*, where $\mathbb{V}(\omega, \mathbf{x})$ is zero. This result does not, however, apply to

$$\mathbb{T}^{-1} = \mathbb{G}_0 + \mathbb{V}^{-1}, \quad (26)$$

because the free Green's function is nonlocal. The potential $\mathbb{V}(\omega, \mathbf{x})$ which appears in Eq. (22) is the coordinate space matrix element of \mathbb{V} , $\langle \mathbf{x} | \mathbb{V} | \mathbf{x}' \rangle = \mathbb{V}(\omega, \mathbf{x}) \delta(\mathbf{x} - \mathbf{x}')$, which can be generalized to the case where \mathbb{V} is non-local, $\langle \mathbf{x} | \mathbb{V} | \mathbf{x}' \rangle = \mathbb{V}(\omega, \mathbf{x}, \mathbf{x}')$. Note that whether \mathbb{V} is local or non-local, its matrix elements vanish if \mathbf{x} and \mathbf{x}' are on different objects or if either \mathbf{x} or \mathbf{x}' is outside of the objects. The definition of \mathbb{V}^{-1} is natural, $\langle \mathbf{x} | \mathbb{V}^{-1} | \mathbf{x}' \rangle = \mathbb{V}^{-1}(\omega, \mathbf{x}) \delta(\mathbf{x} - \mathbf{x}')$ (and similarly for the non-local case) when \mathbf{x} and \mathbf{x}' are on a single object, which is the only case that enters our analysis.

Next we connect the matrix elements of the \mathbb{T} -operator between states with equal ω to the scattering amplitude \mathcal{F} . In our formalism, only this restricted subset of \mathbb{T} -operator matrix elements is needed in the computation of the Casimir energy.

By the choice of the homogeneous solution, $|\mathbf{E}_0\rangle$, is regular or outgoing, we can distinguish two physically different processes. In the former case, the object scatters the regular wave outward and modifies the amplitude of the imposed regular wave

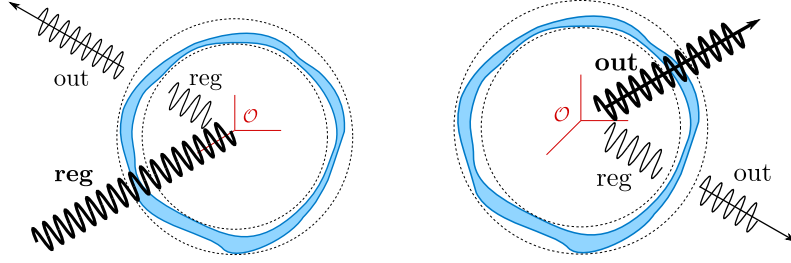


Fig. 3 The scattering waves for outside scattering (left panel) and inside scattering (right panel). In both cases the homogeneous solution $\mathbf{E}_0(\omega)$ is shown in bold. For outside scattering, the homogeneous solution is a regular wave, which produces a regular wave inside the object and an outgoing wave outside the object. For inside scattering, the homogeneous solution is an outgoing wave, which produces a regular wave inside the object and an outgoing wave outside the object.

functions inside, a situation we refer to as outside scattering (left panel of Fig. 3).² In the latter case, the object modifies the amplitude of the transmitted wave and partly reflects it as a regular wave inside (inside scattering, right panel of Fig. 3). ‘Outside’ and ‘inside’ are distinguished by surfaces $\xi_1 = \text{constant}$, as before. Here we treat the *outside scattering case*, and refer the reader to Ref. [75] the *inside case* and further details. The expansion in Eq. (17) allows us to express Eq. (24) as

$$\mathbf{E}(\omega, \mathbf{x}) = \mathbf{E}_\alpha^{\text{reg}}(\omega, \mathbf{x}) - \sum_{\beta} \mathbf{E}_\beta^{\text{out}}(\omega, \mathbf{x}) \quad (27)$$

$$\times \int C_\beta(\omega) \mathbf{E}_\beta^{\text{reg}*}(\omega, \mathbf{x}') \cdot \mathbb{T}(\omega, \mathbf{x}', \mathbf{x}'') \mathbf{E}_\alpha^{\text{reg}}(\omega, \mathbf{x}'') d\mathbf{x}' d\mathbf{x}''.$$

at points \mathbf{x} outside a surface $\xi_1 = \text{constant}$ enclosing the object. The equation can be written in Dirac notation, again with the condition that the domain of the functional Hilbert space is chosen appropriately to the type of solution,

$$|\mathbf{E}(\omega)\rangle = |\mathbf{E}_\alpha^{\text{reg}}(\omega)\rangle + \sum_{\beta} |\mathbf{E}_\beta^{\text{out}}(\omega)\rangle \times \underbrace{(-1)C_\beta(\omega) \langle \mathbf{E}_\beta^{\text{reg}}(\omega) | \mathbb{T}(\omega) | \mathbf{E}_\alpha^{\text{reg}}(\omega) \rangle}_{\mathcal{F}_{\beta,\alpha}^{ee}(\omega)}, \quad (28)$$

which defines $\mathcal{F}_{\beta,\alpha}^{ee}$ as the exterior/exterior scattering amplitude (the one evaluated between two regular solutions). We will use analogous notation in the other cases below.

At coordinates \mathbf{x} “far enough inside” a cavity of the object, meaning that \mathbf{x} has smaller ξ_1 than any point on the object, the field \mathbf{E} is given by

² Alternatively, we can set up asymptotically incoming and outgoing waves on the outside and regular waves inside. The amplitudes of the outgoing waves are then given by the S -matrix, which is related to the scattering amplitude \mathcal{F} by $\mathcal{F} = (S - I)/2$. Although these two matrices carry equivalent information, the scattering amplitude will be more convenient for our calculation.

$$|\mathbf{E}(\omega)\rangle = |\mathbf{E}_\alpha^{\text{reg}}(\omega)\rangle + \sum_\beta |\mathbf{E}_\beta^{\text{reg}}(\omega)\rangle \times \underbrace{(-1)C_\beta(\omega)\langle \mathbf{E}_\beta^{\text{in}}(\omega)|\mathbb{T}(\omega)|\mathbf{E}_\alpha^{\text{reg}}(\omega)\rangle}_{\mathcal{F}_{\beta,\alpha}^{ie}(\omega)}, \quad (29)$$

where again the free states are only defined over the appropriate domain in position space, and \mathcal{F}^{ie} indicates the interior/exterior scattering amplitude.

We have obtained the scattering amplitude in the basis of free solutions with fixed ω . Since one is normally interested in the scattering of waves outside the object, the scattering amplitude usually refers to \mathcal{F}^{ee} . We will use a more general definition, which encompasses all possible combinations of inside and outside. The scattering amplitude is always “on-shell,” because the frequencies of both the operator and the states is ω . As a result, it is a special case of the \mathbb{T} -operator, which can connect wave functions with different ω .

We find it convenient to assemble the scattering amplitudes for inside and outside into a single matrix,

$$\begin{aligned} \mathbb{F}(\kappa) &= \begin{pmatrix} \mathcal{F}^{ee}(\kappa) & \mathcal{F}^{ei}(\kappa) \\ \mathcal{F}^{ie}(\kappa) & \mathcal{F}^{ii}(\kappa) \end{pmatrix} \\ &= (-1)C_\alpha(\kappa) \begin{pmatrix} \langle \mathbf{E}_\alpha^{\text{reg}}(\kappa)|\mathbb{T}(ic\kappa)|\mathbf{E}_\beta^{\text{reg}}(\kappa)\rangle & \langle \mathbf{E}_\alpha^{\text{reg}}(\kappa)|\mathbb{T}(ic\kappa)|\mathbf{E}_\beta^{\text{out}}(\kappa)\rangle \\ \langle \mathbf{E}_\alpha^{\text{in}}(\kappa)|\mathbb{T}(ic\kappa)|\mathbf{E}_\beta^{\text{reg}}(\kappa)\rangle & \langle \mathbf{E}_\alpha^{\text{in}}(\kappa)|\mathbb{T}(ic\kappa)|\mathbf{E}_\beta^{\text{out}}(\kappa)\rangle \end{pmatrix}. \end{aligned} \quad (30)$$

where we have set $\omega = ic\kappa$, since this is the case we use. For simplicity we define

$$\mathcal{F}_{\beta,\alpha}^{ie}(\omega)\Big|_{\omega=ic\kappa} \equiv \mathcal{F}_{\beta,\alpha}^{ie}(ic\kappa).$$

2.4 Casimir free energy in terms of the scattering amplitudes

With the tools of the previous two sections, we are now able to re-express the Euclidean electromagnetic partition function of Eq. (12) in terms of the scattering theory results derived in Section 2.3 for imaginary frequency. We exchange the fluctuating field \mathbf{A} , which is subject to the potential $\mathbb{V}(ic\kappa, \mathbf{x})$, for a free field \mathbf{A}' , together with fluctuating currents \mathbf{J} and charges $-\frac{i}{\omega}\nabla\cdot\mathbf{J}$ that are confined to the objects³

We multiply and divide the partition function Eq. (12) by

$$W = \int \mathcal{D}\mathbf{J}\mathcal{D}\mathbf{J}^*|_{\text{obj}} \exp \left[-\beta \int d\mathbf{x} \mathbf{J}^*(\mathbf{x}) \cdot \mathbb{V}^{-1}(ic\kappa, \mathbf{x}) \mathbf{J}(\mathbf{x}) \right] = \det \mathbb{V}(ic\kappa, \mathbf{x}, \mathbf{x}'), \quad (31)$$

where $|_{\text{obj}}$ indicates that the currents are defined only over the objects, *i.e.* the domain where \mathbb{V} is nonzero and therefore \mathbb{V}^{-1} exists.

³ The sequence of two changes of variables is known as Hubbard-Stratonovich transformation in condensed matter physics.

We then change variables in the integration, $\mathbf{J}(\mathbf{x}) = \mathbf{J}'(\mathbf{x}) + \frac{i}{\kappa} \nabla(ic\kappa, \mathbf{x})\mathbf{E}(\mathbf{x})$, and a second time, $\mathbf{E}(ic\kappa, \mathbf{x}) = \mathbf{E}'(ic\kappa, \mathbf{x}) - i\kappa \int d\mathbf{x}' \mathbb{G}_0(ic\kappa, \mathbf{x}, \mathbf{x}')\mathbf{J}'(\mathbf{x}')$ and analogously for \mathbf{J}^* and \mathbf{E}^* , to obtain

$$Z(\kappa) = \frac{Z_0}{W} \int \mathcal{D}\mathbf{J}' \mathcal{D}\mathbf{J}'^* \Big|_{\text{obj}} \exp \left[-\beta \int d\mathbf{x} d\mathbf{x}' \mathbf{J}'^*(\mathbf{x}) \cdot (\mathbb{G}_0(ic\kappa, \mathbf{x}, \mathbf{x}') + \nabla^{-1}(ic\kappa, \mathbf{x}, \mathbf{x}')) \mathbf{J}'(\mathbf{x}') \right], \quad (32)$$

where

$$Z_0 = \int \mathcal{D}\mathbf{A}' \mathcal{D}\mathbf{A}'^* \exp \left[-\beta \int d\mathbf{x} \mathbf{E}'^*(\mathbf{x}) \cdot \left(\mathbb{I} + \frac{1}{\kappa^2} \nabla \times \nabla \times \right) \mathbf{E}'(\mathbf{x}) \right] \quad (33)$$

is the partition function of the free field, which is independent of the objects. In $Z(\kappa)$, current fluctuations replace the field fluctuations of Eq. (12). The interaction of current fluctuations on different objects is described by the free Green's function $\mathbb{G}_0(ic\kappa, \mathbf{x}, \mathbf{x}')$ alone. The inverse potential penalizes current fluctuations if the potential is small.

To put the partition function into a suitable form for practical computations, we use the results of the previous sections to re-express the microscopic current fluctuations as macroscopic multipole fluctuations, which then can be connected to the individual objects' scattering amplitudes. This transformation comes about naturally once the current fluctuations are decomposed according to the objects on which they occur and the appropriate expansions of the Green's function are introduced. We begin this process by noticing that the operator in the exponent of the integrand in Eq. (32) is the negative of the inverse of the \mathbb{T} -operator (see Eq. (26)), and hence

$$Z(\kappa) = Z_0 \det \nabla^{-1}(ic\kappa, \mathbf{x}, \mathbf{x}') \det \mathbb{T}(ic\kappa, \mathbf{x}, \mathbf{x}') \quad (34)$$

which is in agreement with a more formal calculation: Since $Z_0 = \det \mathbb{G}_0(ic\kappa, \mathbf{x}, \mathbf{x}')$ and $Z(\kappa) = \det \mathbb{G}(ic\kappa, \mathbf{x}, \mathbf{x}')$, we only need to take the determinant of Eq. (25) to arrive at the result of Eq. (34).

Both Z_0 and $\det \nabla^{-1}(ic\kappa, \mathbf{x})$ are independent of the separation of the objects, since the former is simply the free Green's function, while the latter is diagonal in \mathbf{x} . Even a nonlocal potential $\nabla(ic\kappa, \mathbf{x}, \mathbf{x}')$ only connects points within the same object, so its determinant is also independent of the objects' separation. Because these determinants do not depend on separation, they are canceled by a reference partition function in the final result. We are thus left with the task of computing the determinant of the \mathbb{T} -operator.

As has been discussed in Sec. 2.3, the \mathbb{T} -operator $\mathbb{T}(ic\kappa, \mathbf{x}, \mathbf{x}')$ is not diagonal in the spatial coordinates. Its determinant needs to be taken over the spatial indices \mathbf{x} and \mathbf{x}' , which are restricted to the objects because the fluctuating currents $\mathbf{J}(\mathbf{x})$ in the functional integrals are zero away from the objects. This determinant also runs over the ordinary vector components of the electromagnetic \mathbb{T} operator.

A change of basis to momentum space does not help in computing the determinant of the \mathbb{T} -operator, even though it does help in finding the determinant of the free Green's function, for example. One reason is that the momentum basis is not orthogonal over the domain of the indices \mathbf{x} and \mathbf{x}' , which is restricted to the objects. In addition, a complete momentum basis includes not only all directions of the momentum vector, but also all magnitudes of the momenta. So, in the matrix element $\langle \mathbf{E}_{\mathbf{k}} | \mathbb{T}(\omega) | \mathbf{E}_{\mathbf{k}'} \rangle$ the wave numbers k and k' would not have to match, and could also differ from ω/c . That is, the matrix elements could be "off-shell." Therefore, the \mathbb{T} -operator could not simply be treated as if it was the scattering amplitude, which is the on-shell representation of the operator in the subbasis of frequency ω (see Sec. 2.3), and is significantly easier to calculate. Nonetheless, we will see that it is possible to express the Casimir energy in terms of the on-shell operator only, by remaining in the position basis.

From Eq. (25), we know that the inverse of the \mathbb{T} -operator equals the sum of the free Green's function and the inverse of the potential. Since the determinant of the inverse operator is the reciprocal of the determinant, it is expedient to start with the inverse \mathbb{T} -operator. We then separate the basis involving all the objects into blocks for the n objects. In a schematic notation, we have

$$[\langle \mathbf{x} | \mathbb{T}^{-1} | \mathbf{x}' \rangle] = \left(\begin{array}{c|c|c} [\langle \mathbf{x}_1 | \mathbb{T}_1^{-1} | \mathbf{x}'_1 \rangle] & [\langle \mathbf{x}_1 | \mathbb{G}_0 | \mathbf{x}'_2 \rangle] & \cdots \\ \hline [\langle \mathbf{x}_2 | \mathbb{G}_0 | \mathbf{x}'_1 \rangle] & [\langle \mathbf{x}_2 | \mathbb{T}_2^{-1} | \mathbf{x}'_2 \rangle] & \cdots \\ \hline \cdots & \cdots & \cdots \end{array} \right), \quad (35)$$

where the i th submatrix refers to $\mathbf{x} \in$ object i and $\mathbf{x}' \in$ object j and \mathbf{x}_i represents a point in object i measured with respect to some fixed coordinate system. Unlike the position vectors in Sec. 2.2, at this point the subscript of \mathbf{x}_i does not indicate the origin with respect to which the vector is measured, but rather the object on which the point lies. Square brackets are used to remind us that we are considering the entire matrix or submatrix and not a single matrix element. We note that the operators \mathbb{T} and \mathbb{G}_0 are functions of $ic\kappa$, but for simplicity we suppress this argument throughout this derivation. When the two spatial indices lie on different objects, only the free Green's function remains in the off-diagonal submatrices, because $\langle \mathbf{x}_i | \mathbb{V}^{-1} | \mathbf{x}'_j \rangle = 0$ for $i \neq j$.

Next, we multiply \mathbb{T}^{-1} by a reference \mathbb{T} -operator \mathbb{T}_∞ without off-diagonal submatrices, which can be interpreted as the \mathbb{T} -operator at infinite separation,

$$[\langle \mathbf{x} | \mathbb{T}_\infty \mathbb{T}^{-1} | \mathbf{x}'' \rangle] = \left(\begin{array}{c|c|c} [\langle \mathbf{x}_1 | \mathbf{x}''_1 \rangle] & [\int d\mathbf{x}'_1 \langle \mathbf{x}_1 | \mathbb{T}_1 | \mathbf{x}'_1 \rangle \langle \mathbf{x}'_1 | \mathbb{G}_0 | \mathbf{x}''_2 \rangle] & \cdots \\ \hline [\int d\mathbf{x}'_2 \langle \mathbf{x}_2 | \mathbb{T}_2 | \mathbf{x}'_2 \rangle \langle \mathbf{x}'_2 | \mathbb{G}_0 | \mathbf{x}''_1 \rangle] & [\langle \mathbf{x}_2 | \mathbf{x}''_2 \rangle] & \cdots \\ \hline \cdots & \cdots & \cdots \end{array} \right). \quad (36)$$

Each off-diagonal submatrix $[\int d\mathbf{x}'_i \langle \mathbf{x}_i | \mathbb{T}_i | \mathbf{x}'_i \rangle \langle \mathbf{x}'_i | \mathbb{G}_0 | \mathbf{x}''_j \rangle]$ is the product of the \mathbb{T} -operator of object i , evaluated at two points \mathbf{x}_i and \mathbf{x}'_i on that object, multiplied by the free Green's function, which connects \mathbf{x}'_i to some point \mathbf{x}''_j on object j .

Now we shift all variables to the coordinate systems of the objects on which they lie. As a result, the index on a position vector \mathbf{x}_i now refers to the object i on which the point lies *and* to the coordinate system with origin \mathcal{O}_i in which the vector is represented, in agreement with the notation of Sec. 2.2. The off-diagonal submatrices in Eq. (36) can then be rewritten using Eq. (19) as,

$$\sum_{\alpha,\beta} \left[\left(\langle \mathbf{x}_i | \mathbb{T}_i | \mathbf{E}_\alpha^{\text{reg}}(\boldsymbol{\kappa}) \rangle \langle \mathbf{x}_i | \mathbb{T}_i | \mathbf{E}_\alpha^{\text{out}}(\boldsymbol{\kappa}) \rangle \right) \mathbb{X}_{\alpha\beta}^{ij} \begin{pmatrix} \langle \mathbf{E}_\beta^{\text{reg}}(\boldsymbol{\kappa}) | \mathbf{x}_j'' \rangle \\ \langle \mathbf{E}_\beta^{\text{in}}(\boldsymbol{\kappa}) | \mathbf{x}_j'' \rangle \end{pmatrix} (-C_\beta(\boldsymbol{\kappa})) \right]. \quad (37)$$

The matrix $[\langle \mathbf{x} | \mathbb{T}_\infty \mathbb{T}^{-1} | \mathbf{x}'' \rangle]$ has the structure $\mathbb{I} + \mathbb{A}\mathbb{B}$. Using Sylvester's determinant formula $\det(\mathbb{I} + \mathbb{A}\mathbb{B}) = \det(\mathbb{I} + \mathbb{B}\mathbb{A})$, we see that the determinant is unchanged if we replace the off-diagonal submatrices in Eq. (36) by

$$\left[\sum_\beta (-1) C_\alpha(\boldsymbol{\kappa}) \begin{pmatrix} \langle \mathbf{E}_\alpha^{\text{reg}}(\boldsymbol{\kappa}) | \mathbb{T}_i | \mathbf{E}_\beta^{\text{reg}}(\boldsymbol{\kappa}) \rangle \langle \mathbf{E}_\alpha^{\text{reg}}(\boldsymbol{\kappa}) | \mathbb{T}_i | \mathbf{E}_\beta^{\text{out}}(\boldsymbol{\kappa}) \rangle \\ \langle \mathbf{E}_\alpha^{\text{in}}(\boldsymbol{\kappa}) | \mathbb{T}_i | \mathbf{E}_\beta^{\text{reg}}(\boldsymbol{\kappa}) \rangle \langle \mathbf{E}_\alpha^{\text{in}}(\boldsymbol{\kappa}) | \mathbb{T}_i | \mathbf{E}_\beta^{\text{out}}(\boldsymbol{\kappa}) \rangle \end{pmatrix} \mathbb{X}_{\beta,\gamma}^{ij} \right]. \quad (38)$$

With this change, the diagonal submatrices in Eq. (36) become diagonal in the partial wave indices rather than in position space. The matrix elements of the \mathbb{T} -operator are the scattering amplitudes, which can be obtained from ordinary scattering calculations, as demonstrated in Sec. 2.3. The first matrix in Eq. (38), including the prefactor $(-1)C_\alpha(\boldsymbol{\kappa})$, is $\mathbb{F}_i(\boldsymbol{\kappa})$, the modified scattering amplitude of object i , defined in Eq. (30).

Putting together Eqs. (11), (12), (34), and (36), we obtain

$$\mathcal{E} = \frac{\hbar c}{2\pi} \int_0^\infty d\boldsymbol{\kappa} \log \det(\mathbb{M}\mathbb{M}_\infty^{-1}), \quad (39)$$

where

$$\mathbb{M} = \begin{pmatrix} \mathbb{F}_1^{-1} & \mathbb{X}^{12} & \mathbb{X}^{13} & \dots \\ \mathbb{X}^{21} & \mathbb{F}_2^{-1} & \mathbb{X}^{23} & \dots \\ \dots & \dots & \dots & \dots \end{pmatrix} \quad (40)$$

and \mathbb{M}_∞^{-1} is a block diagonal matrix $\text{diag}(\mathbb{F}_1 \ \mathbb{F}_2 \ \dots)$.

Using the block determinant identity

$$\det \begin{pmatrix} \mathbb{A} & \mathbb{B} \\ \mathbb{C} & \mathbb{D} \end{pmatrix} = \det(\mathbb{A}) \det(\mathbb{D} - \mathbb{C}\mathbb{A}^{-1}\mathbb{B}) = \det(\mathbb{D}) \det(\mathbb{A} - \mathbb{B}\mathbb{D}^{-1}\mathbb{C}), \quad (41)$$

we can simplify this expression for the case of the interaction between two objects,

$$\mathcal{E} = \frac{\hbar c}{2\pi} \int_0^\infty d\boldsymbol{\kappa} \log \det \left(\mathbb{I} - \mathbb{F}_a \mathbb{X}^{ab} \mathbb{F}_b \mathbb{X}^{ba} \right). \quad (42)$$

Usually, not all of the submatrices of \mathbb{F} and \mathbb{X} are actually needed for a computation. For example, if all objects are outside of one another, only the submatrices \mathcal{F}^{ee} of the scattering amplitude that describe outside reflection are needed. If there are only two objects, one inside another, then only the inside reflection submatrix \mathcal{F}^{ii}

of the outside object and the outside reflection submatrix \mathcal{F}^{ee} of the inside object are needed.

In order to obtain the free energy at nonzero temperature instead of the ground state energy, we do not take the limit $\beta \rightarrow \infty$ in Eq. (9). Instead, the integral $\frac{\hbar c}{2\pi} \int_0^\infty d\kappa$ is replaced everywhere by $\frac{1}{\beta} \sum'_n$, where $c\kappa_n = \frac{2\pi n}{\hbar\beta}$ with $n = 0, 1, 2, 3, \dots$ is the n th Matsubara frequency. A careful analysis of the derivation shows that the zero frequency mode is weighted by 1/2 compared to the rest of the terms in the sum; this modification of the sum is denoted by a prime on the summation symbol. The factor of 1/2 comes about because the fluctuating charges or currents have to be real for zero frequency. Thus, for κ_0 , the expressions on the right hand side of Eq. (34) should be placed under a square root. (For a complex field, both signs of the integer n would be included separately, and $n = 0$ would be included once, with the normal weight.)

If the medium between the objects is not vacuum but instead has permittivity $\epsilon_M(i\kappa)$ and magnetic permeability $\mu_M(i\kappa)$ different from unity, then the free Green's function is multiplied by $\mu_M(i\kappa)$, and its argument κ is replaced by $n_M(i\kappa)\kappa$, where $n_M(i\kappa) = \sqrt{\epsilon_M(i\kappa)\mu_M(i\kappa)}$ is the medium's index of refraction. Effectively, this change just scales all frequency dependencies in the translation matrices $\mathbb{X}(\kappa)$, which become $\mathbb{X}(n_M(i\kappa)\kappa)$. Furthermore, the scattering amplitudes absorb the factor $\mu_M(i\kappa)$ from the free Green's function and change non-trivially, *i.e.* not just by some overall factor or a scaling of the frequency. They have to be computed with the nonzero electric and magnetic susceptibilities of the medium.

3 Constraints on stable equilibria

Before presenting particular applications of the Casimir energy expression in Eq. (39), we consider some general properties of electrodynamic Casimir interactions here. This section has been adapted from a letter, which is co-authored by two of us [77].

As described in the Introduction, some general statements about the attractive or repulsive nature of Casimir forces can be made on the basis of the relative permittivity and permeability of objects and the medium they are immersed in. But the sign of the force is largely a matter of perspective, since attractive forces can be easily arranged to produce repulsion along a specific direction, *e.g.*, as in Ref. [84]. Instead, we focus on the question of stability, see Fig. 4, which is more relevant to the design and development of MEMs and levitating devices. We find that interactions between objects within the same class of material (as defined in the Introduction) cannot produce stable configurations.

Let us take a step back and consider the question of stability of mechanical equilibria in the realm of electromagnetism. Earnshaw's theorem [26] states that a collection of charges cannot be held in stable equilibrium solely by electrostatic forces. The charges can attract or repel, but cannot be stably levitated. While the stability of matter (due to quantum phenomena) is a vivid reminder of the caveats to this

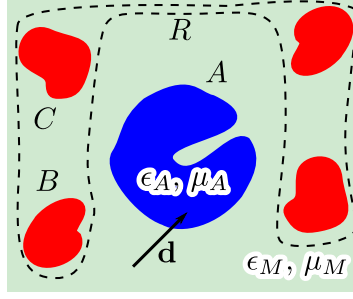


Fig. 4 The Casimir energy is considered for objects with electric permittivity $\varepsilon_i(\omega, \mathbf{x})$ and magnetic permeability $\mu_i(\omega, \mathbf{x})$, embedded in a medium with uniform, isotropic, $\varepsilon_M(\omega)$ and $\mu_M(\omega)$. To study the stability of object A , the rest of the objects are grouped in the combined entity R . The stability of the position of object A is probed by displacing it infinitesimally by vector \mathbf{d} .

theorem, it remains a powerful indicator of the constraints to stability in electrostatics. An extension of Earnshaw's theorem to polarizable objects by Braunbek [9, 8] establishes that dielectric and paramagnetic ($\varepsilon > 1$ and $\mu > 1$) matter cannot be stably levitated by electrostatic forces, while diamagnetic ($\mu < 1$) matter can. This is impressively demonstrated by superconductors and frogs that fly freely above magnets [37]. If the enveloping medium is not vacuum, the criteria for stability are modified by substituting the static electric permittivity ε_M and magnetic permeability μ_M of the medium in place of the vacuum value of 1 in the respective inequalities. In fact, if the medium itself has a dielectric constant higher than the objects ($\varepsilon < \varepsilon_M$), stable levitation is possible, as demonstrated for bubbles in liquids (see Ref. [49], and references therein). For dynamic fields the restrictions of electrostatics do not apply; for example, lasers can lift and hold dielectric beads with index of refraction $n = \sqrt{\varepsilon\mu} > 1$ [1]. In addition to the force which keeps the bead in the center of the laser beam there is radiation pressure which pushes the bead along the direction of the Poynting vector. Ashkin and Gordon have proved that no arrangement of lasers can stably levitate an object just based on radiation pressure [2].

We begin our analysis of equilibria of the electrodynamic Casimir force with the precursor of Eq. (39), which contains the abstract \mathbb{T} and \mathbb{G}_M -operators, where \mathbb{G}_M is the electromagnetic Green's function operator for an isotropic, homogeneous medium,⁴

$$\mathcal{E} = \frac{\hbar c}{2\pi} \int_0^\infty d\kappa \operatorname{tr} \ln \mathbb{T}^{-1} \mathbb{T}_\infty, \quad (43)$$

where the operator $[\mathbb{T}^{-1}(i\kappa, \mathbf{x}, \mathbf{x}')] equals$

⁴ \mathbb{G}_M satisfies $(\nabla \times \mu_M^{-1}(i\kappa) \nabla \times + \varepsilon_M(i\kappa) \kappa^2) \mathbb{G}_M(i\kappa, \mathbf{x}, \mathbf{x}') = \delta(\mathbf{x} - \mathbf{x}') \mathbb{I}$, and is related to G_M , the Green's function of the imaginary frequency Helmholtz equation, by $\mathbb{G}_M(i\kappa, \mathbf{x}, \mathbf{x}') = \mu_M(i\kappa) (\mathbb{I} + (n_M \kappa)^{-2} \nabla \otimes \nabla') G_M(i\kappa, \mathbf{x}, \mathbf{x}')$. Here, $n_M(i\kappa) = \sqrt{\varepsilon_M(i\kappa) \mu_M(i\kappa)}$ is the index of refraction of the medium, whose argument is suppressed to simplify the presentation. Thus \mathbb{G}_M , in contrast to \mathbb{G}_0 , takes into account the permittivity and permeability of the medium when they are different from one.

$$\begin{pmatrix} [\mathbb{T}_A^{-1}(ic\boldsymbol{\kappa}, \mathbf{x}_1, \mathbf{x}'_1)] & [\mathbb{G}_M(ic\boldsymbol{\kappa}, \mathbf{x}_1, \mathbf{x}'_2)] & \cdots \\ [\mathbb{G}_M(ic\boldsymbol{\kappa}, \mathbf{x}_2, \mathbf{x}'_1)] & [\mathbb{T}_B^{-1}(ic\boldsymbol{\kappa}, \mathbf{x}_2, \mathbf{x}'_2)] & \\ \cdots & \cdots & \cdots \end{pmatrix}, \quad (44)$$

and \mathbb{T}_∞ is the inverse of \mathbb{T}^{-1} with \mathbb{G}_M set to zero. The square brackets “[]” denote the entire matrix or submatrix with rows indicated by \mathbf{x} and columns by \mathbf{x}' .⁵ The operator $[\mathbb{T}^{-1}(ic\boldsymbol{\kappa}, \mathbf{x}, \mathbf{x}')]$ has indices in position space. Each spatial index is limited to lie inside the objects A, B, \dots . For both indices \mathbf{x} and \mathbf{x}' in the same object A the operator is just the inverse \mathbb{T} operator of that object, $[\mathbb{T}_A^{-1}(ic\boldsymbol{\kappa}, \mathbf{x}, \mathbf{x}')]$. For indices on different objects, \mathbf{x} in A and \mathbf{x}' in B , it equals the electromagnetic Green’s function operator $[\mathbb{G}_M(ic\boldsymbol{\kappa}, \mathbf{x}, \mathbf{x}')] for an isotropic, homogeneous medium.$

As shown in section 2.4, after a few manipulations, the operators \mathbb{T}_J and \mathbb{G}_M turn into the on-shell scattering amplitude matrix, \mathbb{F}_J , of object J and the translation matrix \mathbb{X} , which converts wave functions between the origins of different objects. While practical computations require evaluation of the matrices in a particular wave function basis, the position space operators \mathbb{T}_J and \mathbb{G}_M are better suited to our general discussion here.

To investigate the stability of object A , we group the ‘rest’ of the objects into a single entity R . So, \mathbb{T} consists of 2×2 blocks, and the integrand in Eq. (43) reduces to $\text{tr} \ln(\mathbb{I} - \mathbb{T}_A \mathbb{G}_M \mathbb{T}_R \mathbb{G}_M)$. Merging the components of R poses no conceptual difficulty given that the operators are expressed in a position basis, while an actual computation of the force between A and R would remain a daunting task. If object A is moved infinitesimally by vector \mathbf{d} , the Laplacian of the energy is given by

$$\nabla_{\mathbf{d}}^2 \mathcal{E} \Big|_{\mathbf{d}=0} = -\frac{\hbar c}{2\pi} \int_0^\infty d\boldsymbol{\kappa} \text{tr} \left[2n_M^2(ic\boldsymbol{\kappa}) \boldsymbol{\kappa}^2 \frac{\mathbb{T}_A \mathbb{G}_M \mathbb{T}_R \mathbb{G}_M}{\mathbb{I} - \mathbb{T}_A \mathbb{G}_M \mathbb{T}_R \mathbb{G}_M} \right. \quad (45)$$

$$\left. + 2\mathbb{T}_A \nabla \mathbb{G}_M \mathbb{T}_R (\nabla \mathbb{G}_M)^T \frac{\mathbb{I}}{\mathbb{I} - \mathbb{T}_A \mathbb{G}_M \mathbb{T}_R \mathbb{G}_M} \right. \quad (46)$$

$$\left. + 2\mathbb{T}_A \nabla \mathbb{G}_M \mathbb{T}_R \mathbb{G}_M \frac{\mathbb{I}}{\mathbb{I} - \mathbb{T}_A \mathbb{G}_M \mathbb{T}_R \mathbb{G}_M} \right. \quad (47)$$

$$\left. \cdot \left(\mathbb{T}_A \nabla \mathbb{G}_M \mathbb{T}_R \mathbb{G}_M + \mathbb{T}_A \mathbb{G}_M \mathbb{T}_R (\nabla \mathbb{G}_M)^T \right) \frac{\mathbb{I}}{\mathbb{I} - \mathbb{T}_A \mathbb{G}_M \mathbb{T}_R \mathbb{G}_M} \right].$$

After displacement of object A , the Green’s function multiplied by \mathbb{T}_A on the left and \mathbb{T}_R on the right ($\mathbb{T}_A \mathbb{G}_M \mathbb{T}_R$) becomes $\mathbb{G}_M(ic\boldsymbol{\kappa}, \mathbf{x} + \mathbf{d}, \mathbf{x}')$, while that multiplied by \mathbb{T}_R on the left and \mathbb{T}_A on the right ($\mathbb{T}_R \mathbb{G}_M \mathbb{T}_A$) becomes $\mathbb{G}_M(ic\boldsymbol{\kappa}, \mathbf{x}, \mathbf{x}' + \mathbf{d})$. The two are related by transposition, and indicated by $\nabla \mathbb{G}_M(ic\boldsymbol{\kappa}, \mathbf{x}, \mathbf{x}') = \nabla_{\mathbf{d}} \mathbb{G}_M(ic\boldsymbol{\kappa}, \mathbf{x} + \mathbf{d}, \mathbf{x}') \Big|_{\mathbf{d}=0}$ and $(\nabla \mathbb{G}_M(ic\boldsymbol{\kappa}, \mathbf{x}, \mathbf{x}'))^T = \nabla_{\mathbf{d}} \mathbb{G}_M(ic\boldsymbol{\kappa}, \mathbf{x}, \mathbf{x}' + \mathbf{d}) \Big|_{\mathbf{d}=0}$ in the above equation. In the first line we have substituted $n_M^2(ic\boldsymbol{\kappa}) \boldsymbol{\kappa}^2 \mathbb{G}_M$ for $\nabla^2 \mathbb{G}_M$; the two differ only by derivatives of δ -functions which vanish since $\mathbb{G}_M(ic\boldsymbol{\kappa}, \mathbf{x}, \mathbf{x}')$ is evaluated with \mathbf{x} in one object and \mathbf{x}' in another. In expressions not containing inverses of \mathbb{T} -operators, we can extend the domain of all operators to the entire space: $\mathbb{T}_J(ic\boldsymbol{\kappa}, \mathbf{x}, \mathbf{x}') = 0$ if \mathbf{x} or \mathbf{x}' are not on object J and thus operator multiplication is unchanged.

⁵ To obtain the free energy at finite temperature, in place of the ground state energy \mathcal{E} , $\int \frac{d\boldsymbol{\kappa}}{2\pi}$ is replaced by the sum $\frac{kT}{\hbar c} \sum'_{\boldsymbol{\kappa}_i \geq 0}$ over Matsubara ‘wavenumbers’ $\boldsymbol{\kappa}_i = 2\pi n kT / \hbar c$ with the $\boldsymbol{\kappa}_0 = 0$ mode weighted by $1/2$.

To determine the signs of the various terms in $\nabla_{\mathbf{d}}^2 \mathcal{E}|_{\mathbf{d}=0}$, an analysis similar to Ref. [51] can be performed. Consequently, the Laplacian of the energy is found to be smaller than or equal to zero as long as both \mathbb{T}_A and \mathbb{T}_R are either positive or negative semidefinite for all imaginary frequencies⁶. The eigenvalues of \mathbb{T}_J , defined in Eq. (25), on the other hand, are greater or smaller than zero depending on the sign s^J of \mathbb{V}_J , since

$$\mathbb{T}_J = s^J \sqrt{s^J \mathbb{V}_J} \frac{\mathbb{I}}{\mathbb{I} + s^J \sqrt{s^J \mathbb{V}_J} \mathbb{G}_M \sqrt{s^J \mathbb{V}_J}} \sqrt{s^J \mathbb{V}_J}. \quad (48)$$

We are left to find the sign of the potential,

$$\begin{aligned} \mathbb{V}_J(ic\kappa, \mathbf{x}) = & \mathbb{I} \kappa^2 (\epsilon_J(ic\kappa, \mathbf{x}) - \epsilon_M(ic\kappa)) \\ & + \nabla \times (\mu_J^{-1}(ic\kappa, \mathbf{x}) - \mu_M^{-1}(ic\kappa)) \nabla \times, \end{aligned} \quad (49)$$

of the object A , and the compound object R ⁷. The sign is determined by the relative permittivities and permeabilities of the objects and the medium: If $\epsilon_J(ic\kappa, \mathbf{x}) > \epsilon_M(ic\kappa)$ and $\mu_J(ic\kappa, \mathbf{x}) \leq \mu_M(ic\kappa)$ hold for all \mathbf{x} in object J , the potential \mathbb{V}_J is positive. If the opposite inequalities are true, \mathbb{V}_J is negative. The curl operators surrounding the magnetic permeability do not influence the sign, as in computing an inner product with \mathbb{V}_J they act symmetrically on both sides. For vacuum $\epsilon_M = \mu_M = 1$, and material response functions $\epsilon(ic\kappa, \mathbf{x})$ and $\mu(ic\kappa, \mathbf{x})$ are analytical continuations of the permittivity and permeability for real frequencies [60]. While $\epsilon(ic\kappa, \mathbf{x}) > 1$ for positive κ , there are no restrictions other than positivity on $\mu(ic\kappa, \mathbf{x})$. (For non-local and non-isotropic response, various inequalities must be generalized to the tensorial operators $\overleftrightarrow{\epsilon}(ic\kappa, \mathbf{x}, \mathbf{x}')$ and $\overleftrightarrow{\mu}(ic\kappa, \mathbf{x}, \mathbf{x}')$.)

Thus, levitation is not possible for collections of objects characterized by $\epsilon_J(ic\kappa, \mathbf{x})$ and $\mu_J(ic\kappa, \mathbf{x})$ falling into one of the two classes described earlier, i) $\epsilon_J/\epsilon_M > 1$ and $\mu_J/\mu_M \leq 1$ (positive \mathbb{V}_J and \mathbb{T}_J), or ii) $\epsilon_J/\epsilon_M < 1$ and $\mu_J/\mu_M \geq 1$ with (negative \mathbb{V}_J and \mathbb{T}_J). (Under these conditions parallel slabs attract.) The frequency and space dependence of the functions has been suppressed in these inequalities. In vacuum, $\epsilon_M(ic\kappa) = \mu_M(ic\kappa) = 1$; since $\epsilon(ic\kappa, \mathbf{x}) > 1$ and the magnetic response of ordinary materials is typically negligible [60], one concludes that stable equilibria of the Casimir force do not exist. If objects A and R , however, belong to different categories — under which conditions the parallel plate force is repulsive — then the terms under the trace in lines (45) and (46) are negative. The positive term in line (47) is typically smaller than the first two, as it involves higher powers of \mathbb{T} and \mathbb{G}_M . In this case stable equilibrium is possible, as demonstrated recently for a small inclusion within a dielectric filled cavity [79]. For the remaining two combinations of inequalities involving ϵ_J/ϵ_M and μ_J/μ_M the sign of \mathbb{V}_J cannot be determined a priori. But for realistic distances between objects and the corresponding frequency

⁶ In practice, \mathbb{T}_A and \mathbb{T}_R suffice to have the same sign over the frequencies, which contribute most to the integral (or the sum) in Eq. (43).

⁷ The first curl in the operator \mathbb{V}_J results from an integration by parts. It is understood that it acts on the wave function multiplying \mathbb{V}_J from the left.

ranges, the magnetic susceptibility is negligible for ordinary materials, and the inequalities involving μ can be ignored.

In summary, the instability theorem applies to all cases where the coupling of the EM field to matter can be described by response functions ε and μ , which may vary continuously with position and frequency. Obviously, for materials which at a microscopic level cannot be described by such response functions, e.g., because of magneto-electric coupling, our theorem is not applicable.

Even complicated arrangements of materials obeying the above conditions are subject to the instability constraint. For example, metamaterials, incorporating arrays of micro-engineered circuitry mimic, at certain frequencies, a strong magnetic response, and have been discussed as candidates for Casimir repulsion across vacuum. (References [87, 86] critique repulsion from dielectric/metallic based metamaterials, in line with our following arguments.) In our treatment, in accord with the usual electrodynamics of macroscopic media, the materials are characterized by $\varepsilon(i\kappa, \mathbf{x})$ and $\mu(i\kappa, \mathbf{x})$ at mesoscopic scales. In particular, chirality and large magnetic response in metamaterials are achieved by patterns made from ordinary metals and dielectrics with well-behaved $\varepsilon(i\kappa, \mathbf{x})$ and $\mu(i\kappa, \mathbf{x}) \approx 1$ at *short* scales. The interesting EM responses merely appear when viewed as ‘effective’ or ‘coarse grained’.

Clearly, the coarse-grained response functions, which are conventionally employed to describe metamaterials, should produce, in their region of validity, the same scattering amplitudes as the detailed mesoscopic description. Consequently, as long as the metamaterial can be described by $\varepsilon(i\kappa, \mathbf{x})$ and $\mu(i\kappa, \mathbf{x}) \approx 1$, the eigenvalues of the \mathbb{T} operators are constrained as described above, and hence subject to the instability theorem. Thus, the proposed use of chiral metamaterials in reference [96] cannot lead to stable equilibrium since the structures are composites of metals and dielectrics. Finally, we note that instability also excludes repulsion between two objects that obey the above conditions, if one of them is an infinite flat plate with continuous translational symmetry: Repulsion would require that the energy as a function of separation from the slab should have $\partial_d^2 \mathcal{E} > 0$ at some point since the force has to vanish at infinite separation. A metamaterial does not have continuous translational symmetry at short length scales but this symmetry is approximately valid in the limit of large separations (long wavelengths), where the material can be effectively described as a homogeneous medium. At short separations lateral displacements might lead to repulsion that, however, must be compatible with the absence of stable equilibrium.

4 Applications

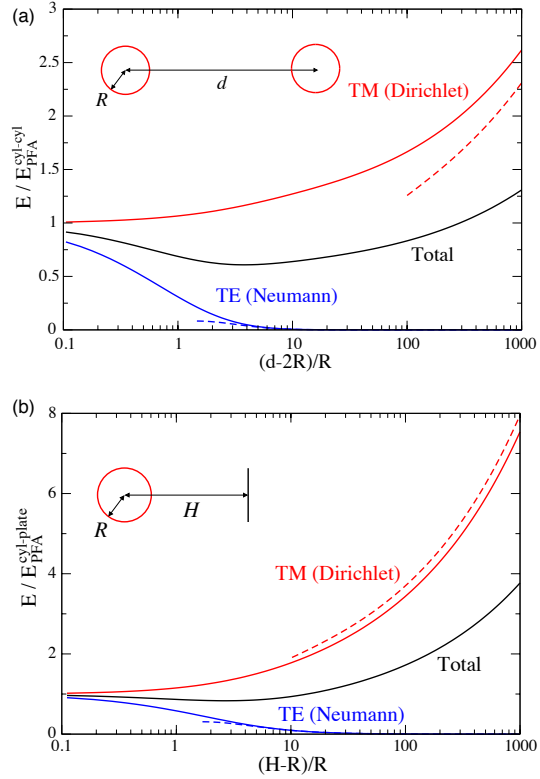
This section gives an overview on different geometries and shapes that have been studied by the approach that we introduced in Section 2. A selection of applications has been made to showcase generic situations and important effects that had not been studied in detail before the development of the methods described here. We

shall mainly summarize analytical and numerical results for the Casimir interaction in the various systems. For details on their derivation and additional implementations of the scattering approach we refer to the literature.

4.1 Cylinders, wires, and plates

The extent to which EM field fluctuations are correlated depends on the effective dimensionality of the space that can be explored by the fluctuations. Therefore, Casimir interactions are expected to depend strongly on the codimension of the interacting objects. The focus of this subsection is on the particular properties of systems with a codimension of the critical value two. We consider these problems in the context of interactions between cylinders and a cylinder and a plate, both perfect reflectors and dielectric materials. Cylindrical geometries are of recent experimental interest since they are easier to hold parallel than plates and still generate a force that is extensive in one direction.

Fig. 5 (a) Casimir energy for two cylinders of equal radius R as a function of surface-to-surface distance $d - 2R$ (normalized by the radius). The energy is divided by the PFA estimate $E_{PFA}^{cyl-cyl}$ for the energy. The solid curves show our numerical results; the dashed lines represent the asymptotic results of Eq. (54). (b) Casimir energy for a cylinder of radius R parallel to a plate as a function of the surface-to-surface distance $H - R$ (normalized by the radius). The energy is divided by the PFA estimate $E_{PFA}^{cyl-plate}$. The solid curves reflect our numerical results; the dashed lines represent the asymptotic results of Eq. (58).



We consider two cylinders of equal radii R and length $L \rightarrow \infty$ with center-to-center separation d , see Fig. 5(a) [76]. (The related configuration where one cylinder is inside another cylinder is treated in reference [22].) For this geometry the interaction energy is obtained from the expression

$$\mathcal{E} = \frac{\hbar c}{2\pi} \int_0^\infty d\kappa \log \det \left(\mathcal{I} - \mathcal{F}_{\text{cyl}}^{ee} \mathcal{W}^{ba} \mathcal{F}_{\text{cyl}}^{ee} \mathcal{W}^{ab} \right). \quad (50)$$

with the exterior scattering amplitudes of a cylinder,

$$\begin{aligned} \mathcal{F}_{\text{cyl},k'_z n' E, k_z n M}^{ee} &= \mathcal{F}_{\text{cyl},k'_z n' M, k_z n E}^{ee} = 0, \\ \mathcal{F}_{\text{cyl},k'_z n' M, k_z n M}^{ee} &= -\frac{2\pi}{L} \delta(k_z - k'_z) \delta_{n,n'} \frac{I'_n(Rp)}{K'_n(Rp)}, \\ \mathcal{F}_{\text{cyl},k'_z n' E, k_z n E}^{ee} &= -\frac{2\pi}{L} \delta(k_z - k'_z) \delta_{n,n'} \frac{I_n(Rp)}{K_n(Rp)}, \end{aligned} \quad (51)$$

and the matrices \mathcal{W}^{ab} , \mathcal{W}^{ba} that translate from cylinder a to b and vice versa. Their elements are summarized in Ref. [75]. The matrix inside the determinant is diagonal in k_z , so the log-determinant over this index turns into an overall integral. A change of variable to polar coordinates converts the integrals over κ and k_z to a single integral over $p = \sqrt{k_z^2 + \kappa^2}$, yielding

$$\mathcal{E} = \frac{\hbar c L}{4\pi} \int_0^\infty p dp (\log \det \mathcal{N}^M + \log \det \mathcal{N}^E), \quad (52)$$

where

$$\begin{aligned} \mathcal{N}_{n,n''}^M &= \delta_{n,n''} - \sum_{n'} \frac{I'_n(pR)}{K'_n(pR)} K_{n+n'}(pd) \frac{I'_{n'}(pR)}{K'_{n'}(pR)} K_{n'+n''}(pd) \\ \mathcal{N}_{n,n''}^E &= \delta_{n,n''} - \sum_{n'} \frac{I_n(pR)}{K_n(pR)} K_{n+n'}(pd) \frac{I_{n'}(pR)}{K_{n'}(pR)} K_{n'+n''}(pd) \end{aligned} \quad (53)$$

describe magnetic (TE) or Neumann modes and electric (TM) or Dirichlet modes, respectively.

For large separations $d \gg R$, the asymptotic behavior of the energy is determined by the matrix elements for $n = n' = 0$ for Dirichlet modes and $n = n' = 0, \pm 1$ for Neumann modes. Taking the determinant of the matrix that consists only of these matrix elements and integrating over p yields straightforwardly the attractive interaction energies

$$\begin{aligned} \mathcal{E}^E &= -\frac{\hbar c L}{d^2} \frac{1}{8\pi \log^2(d/R)} \left(1 - \frac{2}{\log(d/R)} + \dots \right), \\ \mathcal{E}^M &= -\hbar c L \frac{7}{5\pi} \frac{R^4}{d^6} \end{aligned} \quad (54)$$

for electric (Dirichlet) and magnetic (Neumann) modes. The asymptotic interaction is dominated by the contribution from electric (Dirichlet) modes that vanishes for $R \rightarrow 0$ only logarithmically.

For arbitrary separations higher order partial waves have to be considered. The number of partial waves has to be increased with decreasing separation. A numerical evaluation of the determinant and the p -integration can be performed easily and reveals an exponentially fast convergence of the energy in the truncation order for the partial waves. Down to small surface-to-surface separations of $(d - 2R)/R = 0.1$ we find that $n = 40$ partial waves are sufficient to obtain precise results for the energy. The corresponding result for the energies of two cylinders of equal radius is shown in Fig. 5(a). Notice that the minimum in the curve for the total electromagnetic energy results from the scaling by the proximity force approximation (PFA) estimate of the energy. The total energy is monotonic and the force attractive at all separations.

Next we consider a cylinder and an infinite plate, both perfectly reflecting, see Fig. 5(b). The Casimir energy for this geometry has been computed originally in Ref. [33]. In the limit of perfectly reflecting surfaces, the method of images can be employed to compute the Casimir interaction for this geometry [76]. Here we use a different method that can be also applied to real metals or general dielectrics [75]. We express the scattering amplitude of the cylinder now in a plane wave basis, using

$$\mathcal{F}_{\text{cyl}, \mathbf{k}_\perp P, \mathbf{k}'_\perp P'}^{ee} = \sum_{nQ, n'Q'} \frac{C_{\mathbf{k}_\perp P}(\kappa)}{C_Q} D_{\mathbf{k}_\perp P, k_z n Q}^\dagger \mathcal{F}_{\text{cyl}, k_z n Q, k_z n' Q'}^{ee} D_{k_z n' Q', \mathbf{k}'_\perp P'}, \quad (55)$$

where \mathbf{k}_\perp denotes the vector (k_y, k_z) , $C_{\mathbf{k}_\perp P}(\kappa)$ and C_Q are normalization coefficients that can be found together with the matrix elements of the conversion matrix D in Ref. [75]. The elements of the scattering amplitude in the cylindrical basis are given by Eq. (51). The scattering amplitude of the plate is easily expressed in the plane wave basis as

$$\begin{aligned} \mathcal{F}_{\text{plate}, \mathbf{k}'_\perp E, \mathbf{k}_\perp M}^{ee} &= \mathcal{F}_{\text{plate}, \mathbf{k}'_\perp M, \mathbf{k}_\perp E}^{ee} = 0, \\ \mathcal{F}_{\text{plate}, \mathbf{k}'_\perp M, \mathbf{k}_\perp M}^{ee} &= \frac{(2\pi)^2}{L^2} \delta^{(2)}(\mathbf{k}_\perp - \mathbf{k}'_\perp) r^M \left(ic\kappa, \sqrt{1 + \mathbf{k}_\perp^2 / \kappa^2}^{-1} \right), \\ \mathcal{F}_{\text{plate}, \mathbf{k}'_\perp E, \mathbf{k}_\perp E}^{ee} &= \frac{(2\pi)^2}{L^2} \delta^{(2)}(\mathbf{k}_\perp - \mathbf{k}'_\perp) r^E \left(ic\kappa, \sqrt{1 + \mathbf{k}_\perp^2 / \kappa^2}^{-1} \right), \end{aligned} \quad (56)$$

in terms of the Fresnel coefficients that read for a general dielectric surface

$$\begin{aligned} r^M(ic\kappa, x) &= \frac{\mu(ic\kappa) - \sqrt{1 + (n^2(ic\kappa) - 1)x^2}}{\mu(ic\kappa) + \sqrt{1 + (n^2(ic\kappa) - 1)x^2}}, \\ r^E(ic\kappa, x) &= \frac{\varepsilon(ic\kappa) - \sqrt{1 + (n^2(ic\kappa) - 1)x^2}}{\varepsilon(ic\kappa) + \sqrt{1 + (n^2(ic\kappa) - 1)x^2}}. \end{aligned} \quad (57)$$

Here, n is the index of refraction, $n(ic\kappa) = \sqrt{\varepsilon(ic\kappa)\mu(ic\kappa)}$. In the limit of a perfectly reflecting plate one has $r^M \rightarrow -1$, $r^E \rightarrow 1$. The energy given by Eq. (50) can now be evaluated in the plane wave basis with the translation matrices given by the simple expression $\mathcal{W}_{\mathbf{k}_\perp P, \mathbf{k}'_\perp P'}^{ab} = e^{-\sqrt{\mathbf{k}_\perp^2 + \kappa^2} H} \frac{(2\pi)^2}{L^2} \delta^{(2)}(\mathbf{k}_\perp - \mathbf{k}'_\perp) \delta_{P, P'}$.

The asymptotic expression for the attractive interaction energy at large distance $H \gg R$ reads

$$\begin{aligned} \mathcal{E}^E &= -\frac{\hbar c L}{H^2} \frac{1}{16\pi \log(H/R)}, \\ \mathcal{E}^M &= -\hbar c L \frac{5}{32\pi} \frac{R^2}{H^4}. \end{aligned} \quad (58)$$

The total electromagnetic Casimir interaction is again dominated by the contribution from the electric (Dirichlet) mode with $n = 0$ which depends only logarithmically on the cylinder radius. The interaction at all separations follows, as in the case of two cylinders, from a numerical computation of the determinant of Eq. (50) and integration over p . The result is shown in Fig. 5(b).

The above approach has the advantage that it can be also applied to dielectric objects. The scattering amplitude of a dielectric cylinder can be obtained by solving the wave equation in a cylindrical basis with appropriate continuity conditions [75]. The scattering amplitude is diagonal in k_z and the cylindrical wave index n , but not in the polarization. Here we focus on large distances $H \gg R$. Expanding the log det in Eq. (50), we obtain for the interaction energy

$$\mathcal{E} = -\frac{3\hbar c L R^2}{128\pi H^4} \int_0^1 dx \frac{\varepsilon_{\text{cyl},0} - 1}{\varepsilon_{\text{cyl},0} + 1} \left[(7 + \varepsilon_{\text{cyl},0} - 4x^2) r^E(0, x) - (3 + \varepsilon_{\text{cyl},0}) x^2 r^M(0, x) \right], \quad (59)$$

if the zero-frequency magnetic permeability $\mu_{\text{cyl},0}$ of the cylinder is set to one. If we do not set $\mu_{\text{cyl},0}$ equal to one, but instead take the perfect reflectivity limit for the plate, we obtain

$$\mathcal{E} = -\frac{\hbar c L R^2}{32\pi H^4} \frac{(\varepsilon_{\text{cyl},0} - \mu_{\text{cyl},0})(9 + \varepsilon_{\text{cyl},0} + \mu_{\text{cyl},0} + \varepsilon_{\text{cyl},0}\mu_{\text{cyl},0})}{(1 + \varepsilon_{\text{cyl},0})(1 + \mu_{\text{cyl},0})}. \quad (60)$$

Finally, if we let ε_{cyl} be infinite from the beginning (the perfect metal limit for the cylinder), only the $n = 0$ TM mode of the scattering amplitude contributes at lowest order. For a plate with zero-frequency permittivity $\varepsilon_{\text{plate},0}$ and permeability $\mu_{\text{plate},0}$, we obtain for the Casimir energy

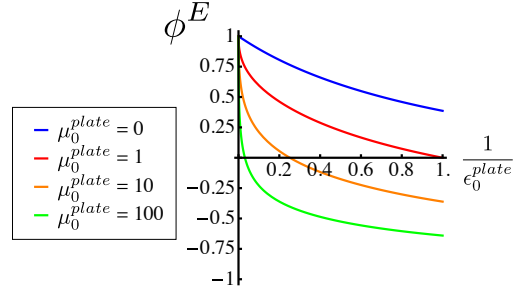
$$\mathcal{E} = \frac{\hbar c L}{16\pi H^2 \log(R/H)} \phi^E, \quad (61)$$

where

$$\phi^E = \int_0^1 \frac{dx}{1+x} \left[r^E(0, x) - x r^M(0, x) \right]. \quad (62)$$

In Fig. 6, ϕ^E is plotted as a function of the zero-frequency permittivity of the plate, $\epsilon_{\text{plate},0}$, for various zero-frequency permeability values, $\mu_{\text{plate},0}$.

Fig. 6 Plots of ϕ^E versus $1/\epsilon_{\text{plate},0}$ for fixed values of $\mu_{\text{plate},0}$. The perfect metal limit ($\phi^E = 1$) is approached slowly for large $\mu_{\text{plate},0}$, as in the case of a sphere opposite a plate. For large $\mu_{\text{plate},0}$ the interaction becomes repulsive, which is expected given similar results for two infinite plates.



4.2 Three-body effects

Casimir interactions are not pair-wise additive. To study the consequences of this property, we consider the case of two identical objects near perfectly reflecting walls [78, 76]. Multibody effects were first observed for such a configuration with two rectangular cylinders sandwiched between two infinite plates by Rodriguez et al. [83]. The role of dimension on this effect is studied by considering either cylinders, see Fig. 7, or spheres, see Fig. 8. While we have given a more detailed description of how the interaction energies follow from the scattering approach in the previous subsection, we mainly provide the final results in this and in the following subsections.

First, we consider the geometry shown in Fig. 7 with two cylinders that are placed parallel to one or in-between two parallel plates, where all objects are assumed to be perfectly reflecting. Using the general expression for the Casimir energy of multiple objects, Eq. (39), the energy can be straightforwardly computed by truncating the matrix \mathbb{M} at a finite partial wave order n . Including up to $n = 35$ partial waves, we obtain for the Casimir force between two cylinders of equal radii in the presence of one or two sidewalls the results shown in Fig. 7. In this figure the force at a fixed surface-to-surface distance $d - 2R = 2R$ between the cylinders is plotted as a function of the relative separation $(H - R)/R$ between the plate and cylinder surfaces. Two interesting features can be observed. First, the attractive total force varies non-monotonically with H : Decreasing for small H and then increasing towards the asymptotic limit between two isolated cylinders for large H , cf. Eq. (54). The extremum for the one-sidewall case occurs at $H - R \approx 0.27R$, and for the two-sidewall case is at $H - R \approx 0.46R$. Second, the total force for the two-sidewall case in the proximity limit $H = R$ is larger than for $H/R \rightarrow \infty$. As might be expected, the H -dependence for one sidewall is weaker than for two sidewalls, and the effects of the

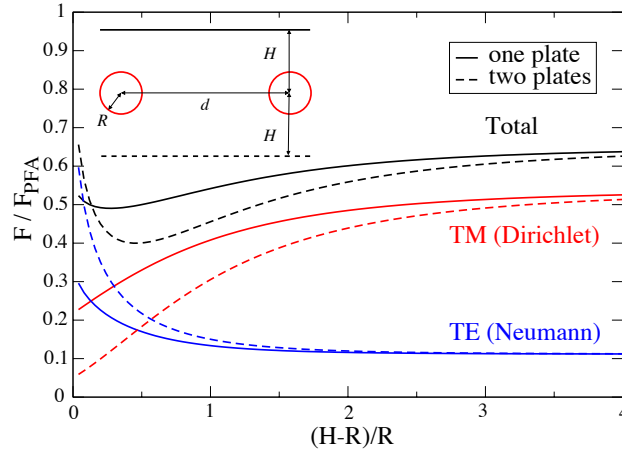


Fig. 7 Electromagnetic Casimir force per unit length between two cylinders of radius R and sidewall separation H vs. the ratio of sidewall separation to cylinder radius $(H - R)/R$, at fixed distance $(d - 2R)/R = 2$ between the cylinders, normalized by the total PFA force per unit length between two isolated cylinders, $F_{\text{PFA}} = \frac{5}{2}(\hbar c \pi^3 / 1920) \sqrt{R/(d - 2R)^7}$. The force is attractive. The solid lines refer to the case with one sidewall, while dashed lines depict the results for two sidewalls. Also shown are the individual TE (blue) and TM (red) forces.

two sidewalls are not additive: not only is the difference from the $H \rightarrow \infty$ force not doubled for two sidewalls compared to one, but the two curves actually intersect at a separation of $H/R = 1.13$. The non-monotonic sidewall effect arises from a competition between the force from TE and TM modes as demonstrated by the results in Fig. 7. The qualitatively different behavior of TE and TM modes can be understood intuitively on the basis of the method of images[76]. The non-monotonicity in H also implies that the force between the cylinders and the sidewalls is not monotonic in d [76].

Second, we replace the two cylinders by two identical, general polarizable compact objects that we specialize later on to spheres [85]. The meaning of the lengths d and H remains unchanged. In dipole approximation, the retarded limit of the interaction is described by the static electric ($\alpha_z, \alpha_{\parallel}$) and magnetic ($\beta_z, \beta_{\parallel}$) dipole polarizabilities of the objects which can be different in the directions perpendicular (z) and parallel (\parallel) to the wall. The well-known Casimir-Polder (CP) potential between two compact objects at large distance is

$$\mathcal{E}_{2,1}(d) = -\frac{\hbar c}{8\pi d^7} \left[33\alpha_{\parallel}^2 + 13\alpha_z^2 - 14\alpha_{\parallel}\beta_z + (\alpha \leftrightarrow \beta) \right]. \quad (63)$$

When a sidewall is added, the energy changes. Its d -dependent part is then

$$\mathcal{E}_{\text{oo}}(d, H) = \mathcal{E}_{2,1}(d) + \mathcal{E}_{2,\setminus}(D, d) + \mathcal{E}_3(D, d) \quad (64)$$

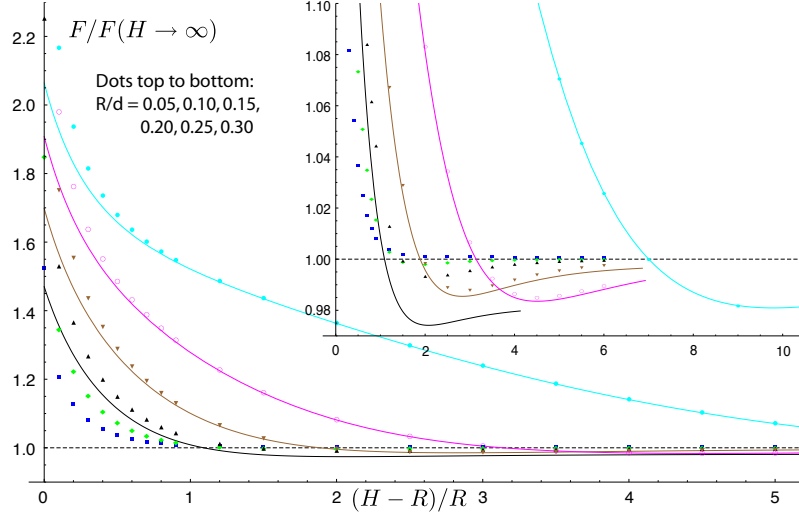


Fig. 8 Electromagnetic Casimir force between two spheres next to one sidewall at separation H vs. the ratio H/R for different sphere separations d . Dotted curves represent numerical results. Shown are also the analytical results of Eq. (68), including terms up to $j = 10$ for $R/d \leq 0.2$ (solid curves) [85]. Inset: Magnification of the nonmonotonicity.

with $D = \sqrt{d^2 + 4H^2}$. The change in the relative orientation of the objects with $\ell = d/D$ leads to a modification of the 2-body CP potential

$$\begin{aligned} \mathcal{E}_{2,\setminus}(D, d) = & -\frac{\hbar c}{8\pi D^7} \left[26\alpha_{\parallel}^2 + 20\alpha_z^2 - 14\ell^2(4\alpha_{\parallel}^2 - 9\alpha_{\parallel}\alpha_z + 5\alpha_z^2) \right. \\ & \left. + 63\ell^4(\alpha_{\parallel} - \alpha_z)^2 - 14(\alpha_{\parallel}\beta_{\parallel}(1 - \ell^2) + \ell^2\alpha_{\parallel}\beta_z) + (\alpha \leftrightarrow \beta) \right]. \end{aligned} \quad (65)$$

The three-body energy $\mathcal{E}_3(D, d)$ describes the collective interaction between the two objects and one image object. It is given by

$$\begin{aligned} \mathcal{E}_3(D, d) = & \frac{4\hbar c}{\pi} \frac{1}{d^3 D^4 (\ell + 1)^5} \left[(3\ell^6 + 15\ell^5 + 28\ell^4 + 20\ell^3 + 6\ell^2 - 5\ell - 1) \right. \\ & \times (\alpha_{\parallel}^2 - \beta_{\parallel}^2) - (3\ell^6 + 15\ell^5 + 24\ell^4 - 10\ell^2 - 5\ell - 1) (\alpha_z^2 - \beta_z^2) \\ & \left. + 4(\ell^4 + 5\ell^3 + \ell^2)(\alpha_z\beta_{\parallel} - \alpha_{\parallel}\beta_z) \right]. \end{aligned} \quad (66)$$

It is instructive to consider the two limits $H \ll d$ and $H \gg d$. For $H \ll d$, \mathcal{E}_{∞} turns out to be the CP potential of Eq. (63) with the replacements $\alpha_z \rightarrow 2\alpha_z$, $\alpha_{\parallel} \rightarrow 0$, $\beta_z \rightarrow 0$, $\beta_{\parallel} \rightarrow 2\beta_{\parallel}$. The two-body and three-body contributions add constructively or destructively, depending on the relative orientation of a dipole and its image which together form a dipole of zero or twice the original strength [85].

For $H \gg d$ the leading correction to the CP potential of Eq. (63) comes from the three-body energy. The energy then becomes (up to order H^{-6})

$$\mathcal{E}_{\underline{\circ}\circ}(d, H) = \mathcal{E}_{2,|}(d) + \frac{\hbar c}{\pi} \left[\frac{\alpha_z^2 - \alpha_{\parallel}^2}{4d^3 H^4} + \frac{9\alpha_{\parallel}^2 - \alpha_z^2 - 2\alpha_{\parallel}\beta_z}{8dH^6} - (\alpha \leftrightarrow \beta) \right]. \quad (67)$$

The signs of the polarizabilities in the leading term $\sim H^{-4}$ can be understood from the relative orientation of the dipole of one object and the image dipole of the other object [85].

Next, we study the case where the two objects are perfectly reflecting spheres of radius R . Now we consider arbitrary distances and include higher order multipole contributions. For $R \ll d, H$ and arbitrary H/d the result for the force can be written as

$$F = \frac{\hbar c}{\pi R^2} \sum_{j=6}^{\infty} f_j(H/d) \left(\frac{R}{d} \right)^{j+2}. \quad (68)$$

The functions f_j can be computed exactly and their full form is given for $j = 6, 7, 8$ in Ref. [85]. For $H \gg d$ one has $f_6(h) = -1001/16 + 3/(4h^6) + \mathcal{O}(h^{-8})$, $f_8(h) = -71523/160 + 39/(80h^6) + \mathcal{O}(h^{-8})$ so that the wall induces weak repulsive corrections. For $H \ll d$, $f_6(h) = -791/8 + 6741h^2/8 + \mathcal{O}(h^4)$, $f_8(h) = -60939/80 + 582879h^2/80 + \mathcal{O}(h^4)$ so that the force amplitude decreases when the spheres are moved a small distance away from the wall. This proves the existence of a minimum in the force amplitude as a function of H for fixed, sufficiently small R/d .

To obtain the interaction at smaller separations or larger radius, the energy $\mathcal{E}_{\underline{\circ}\circ}$ and force $F = -\partial \mathcal{E}_{\underline{\circ}\circ} / \partial d$ between the spheres has been computed numerically [85]. In order to show the effect of the sidewall, the energy and force between the spheres, normalized to the results for two spheres without a wall, is shown in Fig. 8 for fixed d . When the spheres approach the wall, the force first decreases slightly if $R/d \lesssim 0.3$ and then increases strongly under a further reduction of H . For $R/d \gtrsim 0.3$ the force increases monotonically as the spheres approach the wall. This agrees with the prediction of the large distance expansion. The expansion of Eq. (68) with $j = 10$ terms is also shown in Fig. 8 for $R/d \leq 0.2$. Its validity is limited to large d/R and not too small H/R ; it fails completely for $R/d > 0.2$ and hence is not shown in this range.

4.3 Orientation dependence

In this subsection we describe the shape and orientation dependence of the Casimir force using Eq. (39), first reported in Ref. [30]. We consider the orientation dependent force between two spheroids, and between a spheroid and a plane. For two anisotropic objects, the CP potential of Eq. (63) must be generalized. In terms of the Cartesian components of the standard electric (magnetic) polarizability matrix α

(β), the asymptotic large distance potential of two objects (with the \hat{z} axis pointing from one object to the other), can be written as

$$\begin{aligned} \mathcal{E} = & -\frac{\hbar c}{d^7} \frac{1}{8\pi} \left\{ 13 (\alpha_{xx}^1 \alpha_{xx}^2 + \alpha_{yy}^1 \alpha_{yy}^2 + 2\alpha_{xy}^1 \alpha_{xy}^2) \right. \\ & + 20 \alpha_{zz}^1 \alpha_{zz}^2 - 30 (\alpha_{xz}^1 \alpha_{xz}^2 + \alpha_{yz}^1 \alpha_{yz}^2) + (\alpha \rightarrow \beta) \\ & \left. - 7 (\alpha_{xx}^1 \beta_{yy}^2 + \alpha_{yy}^1 \beta_{xx}^2 - 2\alpha_{xy}^1 \beta_{xy}^2) + (1 \leftrightarrow 2) \right\}. \end{aligned} \quad (69)$$

For the case of an ellipsoidal object with static electric permittivity ε and magnetic permeability μ , the polarizability tensors are diagonal in a basis oriented to its principal axes, with elements (for $i \in \{1, 2, 3\}$)

$$\alpha_{ii}^0 = \frac{V}{4\pi} \frac{\varepsilon - 1}{1 + (\varepsilon - 1)n_i}, \quad \beta_{ii}^0 = \frac{V}{4\pi} \frac{\mu - 1}{1 + (\mu - 1)n_i}, \quad (70)$$

where $V = 4\pi r_1 r_2 r_3 / 3$ is the ellipsoid's volume. In the case of spheroids, for which $r_1 = r_2 = R$ and $r_3 = L/2$, the so-called depolarizing factors, n_j , can be expressed in terms of elementary functions, $n_1 = n_2 = \frac{1-n_3}{2}$, $n_3 = \frac{1-e^2}{2e^3} (\log \frac{1+e}{1-e} - 2e)$, where the eccentricity $e = (1 - \frac{4R^2}{L^2})^{1/2}$ is real for a prolate spheroid ($L > 2R$) and imaginary for an oblate spheroid ($L < 2R$). The polarizability tensors for an arbitrary orientation are then obtained as $\alpha = \mathcal{R}^{-1} \alpha^0 \mathcal{R}$, where \mathcal{R} is the matrix that orients the principal axis of the spheroid relative to a fixed Cartesian basis. Note that for rarefied media with $\varepsilon \simeq 1$, $\mu \simeq 1$ the polarizabilities are isotropic and proportional to the volume. Hence, to leading order in $\varepsilon - 1$ the interaction is orientation independent at asymptotically large separations, as we would expect, since pairwise summation is valid for $\varepsilon - 1 \ll 1$. In the following we focus on the interesting opposite limit of two identical perfectly reflecting spheroids. We first consider prolate spheroids with $L \gg R$. The orientation of each "needle" relative to the line joining them (the initial z -axis) is parameterized by the two angles (θ, ψ) , as depicted in Fig. 9(a). Then the energy is

$$\begin{aligned} \mathcal{E}(\theta_1, \theta_2, \psi) = & -\frac{\hbar c}{d^7} \left\{ \frac{5L^6}{1152\pi (\ln \frac{L}{R} - 1)^2} \left[\cos^2 \theta_1 \cos^2 \theta_2 \right. \right. \\ & \left. \left. + \frac{13}{20} \cos^2 \psi \sin^2 \theta_1 \sin^2 \theta_2 - \frac{3}{8} \cos \psi \sin 2\theta_1 \sin 2\theta_2 \right] + \mathcal{O}\left(\frac{L^4 R^2}{\ln \frac{L}{R}}\right) \right\}, \end{aligned} \quad (71)$$

where $\psi \equiv \psi_1 - \psi_2$. It is minimized for two needles aligned parallel to their separation vector. At almost all orientations the energy scales as L^6 , and vanishes logarithmically slowly as $R \rightarrow 0$. The latter scaling changes when one needle is orthogonal to \hat{z} (i.e. $\theta_1 = \pi/2$), while the other is either parallel to \hat{z} ($\theta_2 = 0$) or has an arbitrary θ_2 but differs by an angle $\pi/2$ in its rotation about the z -axis (i.e. $\psi_1 - \psi_2 = \pi/2$). In these cases the energy comes from the next order term in Eq. (71), and takes the

form

$$\mathcal{E}\left(\frac{\pi}{2}, \theta_2, \frac{\pi}{2}\right) = -\frac{\hbar c}{1152\pi d^7} \frac{L^4 R^2}{\ln \frac{L}{R} - 1} (73 + 7 \cos 2\theta_2), \quad (72)$$

which shows that the least favorable configuration corresponds to two needles orthogonal to each other and to the line joining them.

For perfectly reflecting oblate spheroids with $R \gg L/2$, the orientation of each ‘‘pancake’’ is again described by a pair of angles (θ, ψ) , as depicted in Fig. 9(b). To leading order at large separations, the energy is given by

$$\mathcal{E} = -\frac{\hbar c}{d^7} \left\{ \frac{R^6}{144\pi^3} \left[765 - 5(\cos 2\theta_1 + \cos 2\theta_2) + 237 \cos 2\theta_1 \cos 2\theta_2 \right. \right. \\ \left. \left. + 372 \cos 2\psi \sin^2 \theta_1 \sin^2 \theta_2 - 300 \cos \psi \sin 2\theta_1 \sin 2\theta_2 \right] + \mathcal{O}(R^5 L) \right\}. \quad (73)$$

The leading dependence is proportional to R^6 , and does not disappear for any choice of orientations. Furthermore, this dependence remains even as the thickness of the pancake is taken to zero ($L \rightarrow 0$). This is very different from the case of the needles, where the interaction energy vanishes with thickness as $\ln^{-1}(L/R)$. The lack of L dependence is due to the assumed perfect reflectivity. The energy is minimal for two pancakes lying on the same plane ($\theta_1 = \theta_2 = \pi/2$, $\psi = 0$) and has energy $-\hbar c (173/18\pi^3) R^6/d^7$. When the two pancakes are stacked on top of each other, the energy is increased to $-\hbar c (62/9\pi^3) R^6/d^7$. The least favorable configuration is when the pancakes lie in perpendicular planes, i.e., $\theta_1 = \pi/2$, $\theta_2 = 0$, with an energy $-\hbar c (11/3\pi^3) R^6/d^7$.

For an anisotropic object interacting with a perfectly reflecting mirror, at leading order the CP potential is given by

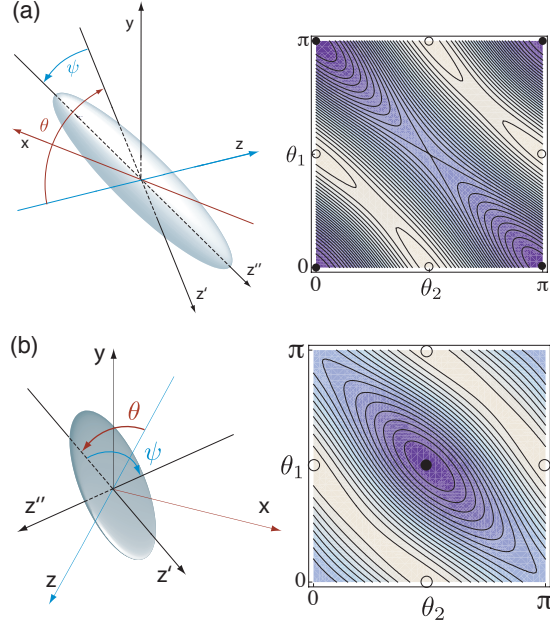
$$\mathcal{E} = -\frac{\hbar c}{d^4} \frac{1}{8\pi} \text{tr}(\alpha - \beta) + \mathcal{O}(d^{-5}), \quad (74)$$

which is clearly independent of orientation. Orientation dependence in this system thus comes from higher multipoles. The next order also vanishes, so the leading term is the contribution from the partial waves with $l = 3$ for which the scattering matrix is not known analytically. However, we can obtain the preferred orientation by considering a distorted sphere in which the radius R is deformed to $R + \delta f(\vartheta, \varphi)$. The function f can be expanded into spherical harmonics $Y_{lm}(\vartheta, \varphi)$, and spheroidal symmetry can be mimicked by choosing $f = Y_{20}(\vartheta, \varphi)$. The leading orientation dependent part of the energy is then obtained as

$$\mathcal{E}_f = -\hbar c \frac{1607}{640\sqrt{5}\pi^{3/2}} \frac{\delta R^4}{d^6} \cos(2\theta). \quad (75)$$

A prolate spheroid ($\delta > 0$) thus minimizes its energy by pointing towards the mirror, while an oblate spheroid ($\delta < 0$) prefers to lie in a plane perpendicular to the mirror. (It is assumed that the perturbative results are not changed for large distortions.)

Fig. 9 (a) Orientation of a prolate (cigar-shaped) spheroid: The symmetry axis (initially the z -axis) is rotated by θ about the x -axis and then by ψ about the z -axis. For two such spheroids, the energy at large distances is given by Eq. (71). The latter is depicted at fixed distance d , and for $\psi_1 = \psi_2$, by a contour plot as function of the angles θ_1, θ_2 for the x -axis rotations. Minima (maxima) are marked by filled (open) dots. (b) As in (a) for oblate (pancake-shaped) spheroids, with a contour plot of energy at large separations.



These configurations are also preferred at small distances d , since (at fixed distance to the center) the object reorients to minimize the closest separation. Interestingly, the latter conclusion is not generally true. In Ref. [30] it has been shown that there can be a transition in preferred orientation as a function of d in the simpler case of a scalar field with Neumann boundary conditions. The separation at which this transition occurs varies with the spheroid's eccentricity.

4.4 Edge and finite size effects

In this subsection, based on work reported in Ref. [45], it is demonstrated that *parabolic* cylinders provide another example where the scattering amplitudes can be computed exactly. We use the exact results for scattering from perfect mirrors to compute the Casimir force between a parabolic cylinder and a plate. In the limiting case when the curvature at its tip vanishes, the parabolic cylinder becomes a semi-infinite plate (a knife's edge), and we can consider how edges and finite size effects influence the Casimir energy.

The surface of a parabolic cylinder in Cartesian coordinates is described by $y = (x^2 - R^2)/2R$ for all z , as shown in Fig. 10(a), where R is the curvature at the tip. In parabolic cylinder coordinates, defined through $x = \mu\lambda$, $y = (\lambda^2 - \mu^2)/2$, $z = z$, the surface is simply $\mu = \mu_0 = \sqrt{R}$ for $-\infty < \lambda, z < \infty$. Since sending $\lambda \rightarrow -\lambda$ and $\mu \rightarrow -\mu$ returns us to the same point, we restrict our attention to $\mu \geq 0$ while considering

all values of λ . Then μ plays the role of the “radial” coordinate in scattering theory and one can again define regular and outgoing waves [45]. Since both objects are perfect mirrors, translational symmetry along the z -axis enables us to decompose the electromagnetic field into two scalar fields, as in the case of circular cylinders in Subsection 4.1. Each scalar field, describing E (Dirichlet) or M (Neumann) modes, can then be treated independently, with the sum of their contributions giving the full electromagnetic result.

The scattering amplitude of the plate is expressed in a plane wave basis and is given by Eq. (56) with $r^M = -1$ and $r^E = 1$. The scattering amplitude of the parabolic cylinder for E and M polarization is obtained in a parabolic cylinder wave basis as [45]

$$\begin{aligned}\mathcal{F}_{\text{para},k_z v E, k'_z v' E}^{ee} &= -\frac{2\pi}{L} \delta(k_z - k'_z) \delta_{v,v'} f_{k_z v E}, & f_{k_z v E} &= i^v \frac{D_v(i\tilde{\mu}_0)}{D_{-v-1}(\tilde{\mu}_0)} \\ \mathcal{F}_{\text{para},k_z v M, k'_z v' M}^{ee} &= -\frac{2\pi}{L} \delta(k_z - k'_z) \delta_{v,v'} f_{k_z v M}, & f_{k_z v M} &= i^{v+1} \frac{D'_v(i\tilde{\mu}_0)}{D'_{-v-1}(\tilde{\mu}_0)},\end{aligned}\quad (76)$$

with $\tilde{\mu}_0 = \sqrt{2R\sqrt{\kappa^2 + k_z^2}}$ and the parabolic cylinder function $D_v(u)$ for integer v .

For the present geometry, the general formula for the Casimir energy per unit length can be expressed explicitly as

$$\frac{\mathcal{E}}{\hbar c L} = \int_0^\infty \frac{d\kappa}{2\pi} \int_{-\infty}^\infty \frac{dk_z}{2\pi} \log \det \left(\delta_{v,v'} - f_{k_z v P} \int_{-\infty}^\infty dk_x \mathcal{U}_{v k_x k_z}(d, \theta) r^P \mathcal{U}_{v' k_x k_z}(d, -\theta) \right) \quad (77)$$

for polarization $P = E$ or M . Here the matrix \mathcal{U} with elements

$$\mathcal{U}_{v k_x k_z}(d, \theta) = \sqrt{\frac{i}{2k_y v! \sqrt{2\pi}}} \left(\frac{\tan \frac{\phi + \theta}{2}}{\cos \frac{\phi + \theta}{2}} \right)^v e^{i k_y d} \quad (78)$$

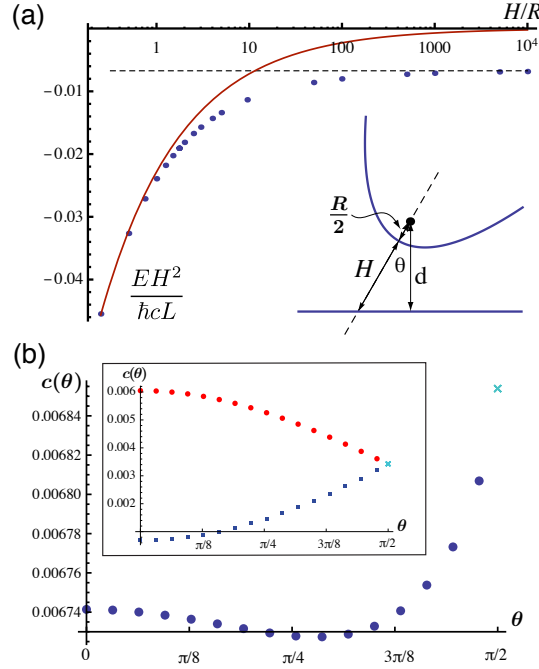
with $k_y = i\sqrt{\kappa^2 + k_x^2 + k_z^2}$ and $\tan \phi = k_x/k_y$, describes the translation from parabolic cylinder to plane waves over the distance d from the focus of the parabola to the plane where θ is the angle of inclination of the parabolic cylinder.

Numerical computations of the energy are performed by truncating the determinant at index v_{\max} . For the numbers quoted below, we have computed for v_{\max} up to 200 and then extrapolated the result for $v_{\max} \rightarrow \infty$, and in Fig. 10 we have generally used $v_{\max} = 100$. The dependence of the energy on the separation $H = d - R/2$ for $\theta = 0$ is shown in Fig. 10(a). At small separations ($H/R \ll 1$) the proximity force approximation, given by

$$\frac{\mathcal{E}_{\text{pfa}}}{\hbar c L} = -\frac{\pi^2}{720} \int_{-\infty}^\infty \frac{dx}{[H + x^2/(2R)]^3} = -\frac{\pi^3}{960\sqrt{2}} \sqrt{\frac{R}{H^5}}, \quad (79)$$

should be valid. The numerical results in Fig. 10(a) indeed confirm this expectation.

Fig. 10 (a) Energy $\mathcal{E}H^2/(\hbar cL)$ versus H/R for $\theta = 0$ and $R = 1$ on a log-linear scale for the parabolic cylinder-plane geometry. The dashed line gives the $R = 0$ limit and the solid curve gives the PFA result. (b) The coefficient $c(\theta)$ as a function of angle for $R = 0$. The exact result at $\theta = \pi/2$ is marked with a cross. Inset: Dirichlet (circles) and Neumann (squares) contributions to the full electromagnetic result.



A more interesting limit is obtained when $R/H \rightarrow 0$, corresponding to a semi-infinite plate for which the PFA energy vanishes. The exact result for the energy for $R = 0$ and $\theta = 0$ is

$$\frac{\mathcal{E}}{\hbar cL} = -\frac{C_{\perp}}{H^2}, \quad (80)$$

where $C_{\perp} = 0.0067415$ is obtained by numerical integration. When the semi-infinite plate is tilted by an angle θ , dimensional analysis suggest for the Casimir energy [39, 92]

$$\frac{\mathcal{E}}{\hbar cL} = -\frac{C(\theta)}{H^2}. \quad (81)$$

The function $c(\theta) = \cos(\theta)C(\theta)$ is shown in Fig. 10(b). A particularly interesting limit is $\theta \rightarrow \pi/2$, when the two plates are parallel. In this case, the leading contribution to the Casimir energy should be proportional to the area of the half-plane according to the parallel plate formula, $E_{\parallel}/(\hbar cA) = -c_{\parallel}/H^3$ with $c_{\parallel} = \pi^2/720$, plus a subleading correction due to the edge. Multiplying by $\cos \theta$ removes the divergence in the amplitude $C(\theta)$ as $\theta \rightarrow \pi/2$. As in [39], we assume $c(\theta \rightarrow \pi/2) = c_{\parallel}/2 + (\theta - \pi/2)c_{\text{edge}}$, although we cannot rule out the possibility of additional non-analytic forms, such as logarithmic or other singularities. With this assumption, we can estimate the edge correction $c_{\text{edge}} = 0.0009$ from the data in Fig. 10(b). From the inset in Fig. 10(b), we estimate the Dirichlet and Neumann contributions to this result to be $c_{\text{edge}}^D = -0.0025$ and $c_{\text{edge}}^N = 0.0034$, respectively. For extensions to other

geometries with edges, inclusion of thermal fluctuations and experimental implications, see Ref. [45].

4.5 Interior configurations

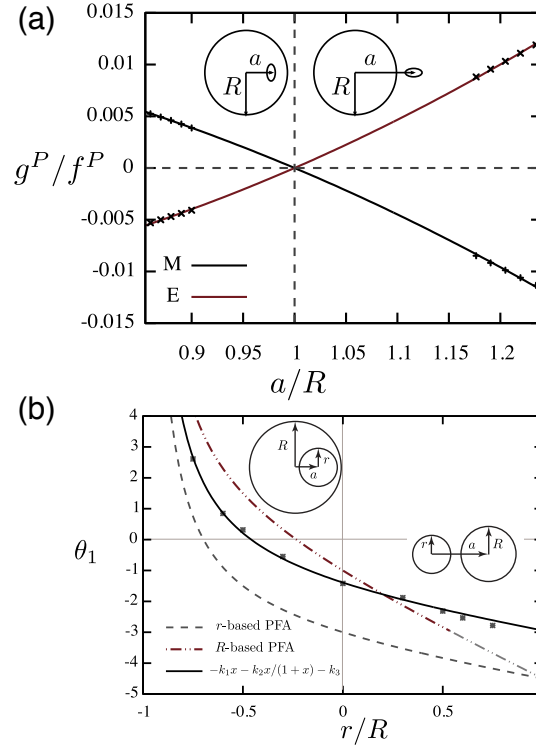
In this last subsection we consider so-called interior configurations where one object is contained within another that can be also studied with the methods introduced in Sect. 2. Specifically, we obtain the electrodynamic Casimir interaction of a conducting or dielectric object inside a perfectly conducting spherical cavity [95]. In the case where an object, i , lies inside a perfectly conducting cavity, the outer object o , the Casimir energy of Eq. (42) becomes

$$\mathcal{E} = \frac{\hbar c}{2\pi} \int_0^\infty d\kappa \log \frac{\det(\mathcal{I} - \mathcal{F}_o^{ii} \mathcal{W}^{io} \mathcal{F}_i^{ee} \mathcal{V}^{io})}{\det(\mathcal{I} - \mathcal{F}_o^{ii} \mathcal{F}_i^{ee})}, \quad (82)$$

where \mathcal{F}_o^{ii} is the scattering amplitude for interior scattering of the conducting cavity, a sphere in our case, and \mathcal{F}_i^{ee} the scattering amplitude of the interior object. The amplitude matrix for interior scattering is the inverse of the corresponding exterior matrix. These scattering amplitudes are evaluated in a spherical vector wave basis with respect to appropriately chosen origins within each object. The translation matrices, \mathcal{W}^{io} and \mathcal{V}^{io} , relate regular wave functions between the coordinate systems of the interior object and the spherical cavity, see Ref. [75] for details. The determinant in the denominator of Eq. (82) subtracts the Casimir energy when the origins of the two objects coincide. This way of normalizing the Casimir energy differs from the exterior cases considered before, where the objects are removed to infinite separation; a choice that would be unnatural in the interior case.

First, we determine the forces and torques on a small object, dielectric or conducting, well separated from the cavity walls. This is the interior analogue of the famous Casimir-Polder force on a polarizable molecule near a perfectly conducting plate [15]. In this case the first term in a multiple scattering expansion, where the integrand of Eq. (82) is replaced by $-\text{Tr}(\mathcal{F}_o^{ii} \mathcal{W}^{io} \mathcal{F}_i^{ee} \mathcal{V}^{io})$, already gives an excellent approximation to the energy. Since the object is small, the scattering amplitude $\mathcal{F}_{i,lmP,l'm'P'}^{ee}$, (where l and m are angular momentum indices and P labels M or E polarization) can be expanded in powers of κ . Only the following terms contribute to lowest order: $\mathcal{F}_{i,1mP,1m'P}^{ee}(\kappa) = 2\kappa^3 \alpha_{mm'}^P / 3 + O(\kappa^4)$, where $\alpha_{mm'}^P$ is the static electric ($P = E$) or magnetic ($P = M$) polarizability tensor of the inner object. We consider an exterior spherical shell of radius R and define a to be the displacement of the center of the interior object from the center of the shell. Using the dipole approximation for the inner object but including all multipoles of the exterior shell, we find for the Casimir energy to leading order in r/R (where r is the typical length scale of the interior object), the energy

Fig. 11 (a) The ratio g^P/f^P , which determines the preferred orientation of the interior object, plotted versus $x = a/R$ showing the change in preferred orientation from interior ($a/R < 1$) to exterior ($a/R > 1$) (displayed by two small ellipses as described in the text). The solid curves are fits of the form $c_1(1-x) + c_2(1-x)^2$ to these data points. (b) PFA correction coefficients for spheres. r/R ranges from -1 (interior concentric), to zero (sphere-plane), to $+1$ (exterior, equal radii). The data points correspond to the exact values of θ_1 calculated numerically, while the solid black curve is a fit (see text). Inset: “interior” and “exterior” geometrical configurations.



$$\begin{aligned} \frac{3\pi R^4}{\hbar c} \mathcal{E}(a/R) &= [f^E(a/R) - f^E(0)] \text{Tr} \alpha^E \\ &+ g^E(a/R)(2\alpha_{zz}^E - \alpha_{xx}^E - \alpha_{yy}^E) + (E \leftrightarrow M). \end{aligned} \quad (83)$$

The z -axis is oriented from the center of the shell to the interior object, and α_{ij}^P represent the interior object’s static polarizability tensors in a Cartesian basis. The coefficient functions f^P and g^P can be obtained in terms of an integral over modified Bessel functions, see Ref. [95]. f^E is negative and decreasing with a/R , while f^M is positive and increasing. There are important differences between Eq. (83) and the classic Casimir-Polder result: first, the energy depends in a non-trivial way on a/R ; second, at any non-zero distance from the center, the interior object experiences a torque; and third, the force between the two bodies depends on the interior object’s orientation.

To explore the orientation dependence of Eq. (83) assume, for simplicity, there is a single frame in which both α^E and α^M are diagonal. In this body-fixed frame, write $\alpha_{xx}^0 - \alpha_{yy}^0 = \beta$ and $\alpha_{zz}^0 - \frac{1}{2}(\alpha_{xx}^0 + \alpha_{yy}^0) = \gamma$ (where we have suppressed the M/E label). The polarizability in the “lab frame” is obtained by $\alpha = \mathcal{R}\alpha^0\mathcal{R}^{-1}$, where \mathcal{R} is a rotation matrix that orients the principal axes of the inner object with respect to the lab frame. This procedure leaves $\text{Tr}\alpha^0$ invariant, and gives for the second line in

Eq. (83),

$$\sum_{P=M,E} g^P(a/R) \left(\frac{3\beta^P}{2} \sin^2 \theta \cos 2\phi + \gamma^P (3 \cos^2 \theta - 1) \right),$$

where ϕ corresponds to the azimuthal rotation of the object about its principal z -axis, and θ is the angle between the object's principal z -axis and the "laboratory" z -axis connecting the center of the sphere to the origin of the interior object.

If $\beta \neq 0$ then the object held at fixed inclination, θ , experiences a torque that causes it to rotate about the body-fixed z -axis. If, however, the object has axial symmetry ($\beta = 0$), then the only torque on the object tries to align it either parallel or perpendicular to the displacement axis.

A "cigar shaped" object ($\gamma > 0$) prefers to orient so as to point perpendicular to the z axis, and a "pancake" ($\gamma < 0$) tries to align its two large axes perpendicular to the z axis. The small ellipse inside the sphere in Fig. 11(a) illustrates a side view of both the cigar and the pancake in their preferred orientation. It is interesting to note that g^E and g^M are both positive. So, in contrast to the force, the contributions to the torque from magnetic and electric polarizabilities are in the same direction, if they have the same sign. More complicated behavior is possible if, for example, the electric and magnetic polarizabilities are not diagonal in the same body-fixed coordinate system. Note that our results cannot be compared to the PFA approximation since the size of the inner object, not the separation of surfaces, d , has been assumed to be the smallest scale in the analysis.

An identical analysis can be performed for a polarizable object outside a metallic sphere where $a/R > 1$. It turns out that the analogous exterior function $g(a/R) < 0$ for both polarizations. Therefore, the preferred orientation of a polarizable object outside a metallic sphere is opposite of that in the interior case (see the small ellipse outside the large sphere in Fig. 11(a)). The continuation of the functions f and g from "interior" to "exterior" is displayed in Fig. 11(a), where the transition from one orientation to the other is clear.

Second, we compute numerically from Eq. (82) the interaction energy of a finite-size metal sphere with the cavity walls when the separation, d , between their surfaces tends to zero. In this limit the Casimir force F between two conducting spheres, which is attractive, is proportional in magnitude to d^{-3} , where $d = R - r - a$ is the separation of surfaces. The coefficient of d^{-3} is given by the PFA,

$$\lim_{d \rightarrow 0} d^3 F = -\frac{\pi^3 \hbar c}{360} \frac{rR}{r+R}. \quad (84)$$

This result holds for both the interior and the exterior configuration of two spheres. For fixed r we formally distinguish the cases: $R > 0$ for the exterior, $R \rightarrow \infty$ for the plate-sphere, and $R < 0$ for the interior configuration, see Fig. 11(b). All possible configurations are taken into account by considering $-1 \leq r/R \leq 1$. Although we know of no derivation of the functional form of the Casimir force beyond the leading term in the PFA, our numerical results are well fit by a power series in d/r ,

$$F = -\frac{\pi^3 \hbar c}{360 d^3} \frac{rR}{r+R} \left(1 + \theta_1(r/R) \frac{d}{2r} - \theta_2(r/R) \frac{d^2}{2r^2} + \dots \right) \quad (85)$$

We have used this functional form to extract the coefficient $\theta_1(r/R)$.

Although the PFA is accurate only in the limit $d/r \rightarrow 0$, it can be extended in various ways to the whole range of d , r , and R . Depending on the surface O from which the normal distance to the other surface is measured, one obtains the “ O -based” PFA energy. Clearly, the result depends on which object one chooses as O , but the various results do agree to leading order in d/r . We can choose either of the two spheres to arrive at the “ r -based PFA” or the “ R -based PFA”, see Fig. 11(b). Either one yields a ‘correction’ to the leading order PFA,

$$\theta_{1,r}^{\text{PFA}}(x) = -\left(x + \frac{x}{1+x} + 3\right), \quad \theta_{1,R}^{\text{PFA}} = -\left(3x + \frac{x}{1+x} + 1\right),$$

where $x = r/R$. In Fig. 11(b) we plot the values of θ_1 extracted from a numerical evaluation of the force from Eq. (82) for various values of $r/R < 0$. For reference, the two PFA estimates are also shown.

The numerical data in Fig. 11(b) show a smooth transition from the interior to the exterior configuration. Although the PFA estimates do not describe the data, the r -based PFA has a similar functional form and divergence as $x \rightarrow -1$. Therefore, we fit the data in Fig. 11(b) to a function, $\theta_1(x) = -(k_1 x + k_2 x / (1+x) + k_3)$ and find, $k_1 = 1.05 \pm 0.14$, $k_2 = 1.08 \pm 0.08$, $k_3 = 1.38 \pm 0.06$. Notice, however, that the actual function $\theta_1(x)$ is not known analytically and that the fit represents a reasonable choice which may not be unique. Our results show that the correction to the PFA has a significant dependence on ratio of curvatures of the two surfaces.

Acknowledgements The research presented here was conducted together with Noah Graham, Steven G. Johnson, Mehran Kardar, Alejandro W. Rodriguez, Pablo Rodriguez-Lopez, Alexander Shpunt, and Saad Zaheer, whom we thank for their collaboration. This work was supported by the National Science Foundation (NSF) through grant DMR-08-03315 (SJR), by the DFG through grant EM70/3 (TE) and by the U. S. Department of Energy (DOE) under cooperative research agreement #DF-FC02-94ER40818 (RLJ).

References

1. Ashkin, A.: Acceleration and Trapping of Particles by Radiation Pressure. *Phys. Rev. Lett.* **24**, 156–159 (1970)
2. Ashkin, A., Gordon, J.P.: Stability of radiation-pressure particle traps: an optical Earnshaw theorem. *Opt. Lett.* **8**, 511–513 (1983)
3. Bachas, C.P.: Comment on the sign of the Casimir force. *J. Phys. A: Math. Theor.* **40**, 9089–9096 (2007)
4. Balian, R., Duplantier, B.: Electromagnetic waves near perfect conductors. II. Casimir effect. *Ann. Phys., NY* **104**, 300–335 (1977)
5. Balian, R., Duplantier, B.: Electromagnetic waves near perfect conductors. I. Multiple scattering expansions. Distribution of modes. *Ann. Phys., NY* **112**, 165–208 (1978)

6. Birman, M.S., Krein, M.G.: On the theory of wave operators and scattering operators. *Sov. Math.-Dokl.* **3**, 740–744 (1962)
7. Bordag, M., Robaschik, D., Wieczorek, E.: Quantum field theoretic treatment of the casimir effect. *Ann. Phys., NY* **165**, 192–213 (1985)
8. Braunbek, W.: Freies Schweben diamagnetischer Körper im Magnetfeld. *Z. Phys.* **112**, 764–769 (1939)
9. Braunbek, W.: Freischwebende Körper im elektrischen und magnetischen Feld. *Z. Phys.* **112**, 753–763 (1939)
10. Bulgac, A., Magierski, P., Wirzba, A.: Scalar Casimir effect between Dirichlet spheres or a plate and a sphere. *Phys. Rev. D* **73**, 025007 (2006)
11. Bulgac, A., Wirzba, A.: Casimir Interaction among Objects Immersed in a Fermionic Environment. *Phys. Rev. Lett.* **87**, 120404 (2001)
12. Büscher, R., Emig, T.: Geometry and Spectrum of Casimir Forces. *Phys. Rev. Lett.* **94**, 133901 (2005)
13. Capasso, F., Munday, J.N., Iannuzzi, D., Chan, H.B.: Casimir Forces and Quantum Electrodynamical Torques: Physics and Nanomechanics. *IEEE J. Sel. Top. Quant.* **13**, 400–414 (2007)
14. Casimir, H.B.G.: On the attraction between two perfectly conducting plates. *Proc. K. Ned. Akad. Wet.* **51**, 793–795 (1948)
15. Casimir, H.B.G., Polder, D.: The Influence of Retardation on the London-van der Waals Forces. *Phys. Rev.* **73**, 360–372 (1948)
16. Chan, H.B., Aksyuk, V.A., Kleiman, R.N., Bishop, D.J., Capasso, F.: Quantum Mechanical Actuation of Microelectromechanical Systems by the Casimir Force. *Science* **291**, 1941–1944 (2001)
17. Chan, H.B., Bao, Y., Zou, J., Cirelli, R.A., Klemens, F., Mansfield, W.M., Pai, C.S.: Measurement of the Casimir Force between a Gold Sphere and a Silicon Surface with Nanoscale Trench Arrays. *Phys. Rev. Lett.* **101**, 030401 (2008)
18. Chen, F., Klimchitskaya, G.L., Mostepanenko, V.M., Mohideen, U.: Demonstration of the Difference in the Casimir Force for Samples with Different Charge-Carrier Densities. *Phys. Rev. Lett.* **97**, 170402 (2006)
19. Chen, F., Klimchitskaya, G.L., Mostepanenko, V.M., Mohideen, U.: Control of the Casimir force by the modification of dielectric properties with light. *Phys. Rev. B* **76**, 035338 (2007)
20. Chen, F., Mohideen, U., Klimchitskaya, G.L., Mostepanenko, V.M.: Demonstration of the Lateral Casimir Force. *Phys. Rev. Lett.* **88**, 101801 (2002)
21. Chew, W.C., Jin, J.M., Michielssen, E., Song, J.M. (eds.): *Fast and Efficient Algorithms in Computational Electrodynamics*. Artech House, Norwood, MA (2001)
22. Dalvit, D.A.R., Lombardo, F.C., Mazzitelli, F.D., Onofrio, R.: Exact Casimir interaction between eccentric cylinders. *Phys. Rev. A* **74**, 020101(R) (2006)
23. Decca, R.S., López, D., Fischbach, E., Klimchitskaya, G.L., Krause, D.E., Mostepanenko, V.M.: Tests of new physics from precise measurements of the Casimir pressure between two gold-coated plates. *Phys. Rev. D* **75**, 077101 (2007)
24. Druzhinina, V., DeKieviet, M.: Experimental Observation of Quantum Reflection far from Threshold. *Phys. Rev. Lett.* **91**, 193202 (2003)
25. Dzyaloshinskii, I.E., Lifshitz, E.M., Pitaevskii, L.P.: The general theory of van der Waals forces. *Adv. Phys.* **10**, 165–209 (1961)
26. Earnshaw, S.: On the Nature of the Molecular Forces which Regulate the Constitution of the Luminiferous Ether. *Trans. Camb. Phil. Soc.* **7**, 97–112 (1842)
27. Ederth, T.: Template-stripped gold surfaces with 0.4-nm rms roughness suitable for force measurements: Application to the Casimir force in the 20–100-nm range. *Phys. Rev. A* **62**, 062104 (2000)
28. Emig, T., Graham, N., Jaffe, R.L., Kardar, M.: Casimir Forces between Arbitrary Compact Objects. *Phys. Rev. Lett.* **99**, 170403 (2007)
29. Emig, T., Graham, N., Jaffe, R.L., Kardar, M.: Casimir forces between compact objects: The scalar case. *Phys. Rev. D* **77**, 025005 (2008)
30. Emig, T., Graham, N., Jaffe, R.L., Kardar, M.: Orientation dependence of Casimir forces. *Phys. Rev. A* **79**, 054901 (2009)

31. Emig, T., Hanke, A., Golestanian, R., Kardar, M.: Probing the Strong Boundary Shape Dependence of the Casimir Force. *Phys. Rev. Lett.* **87**, 260402 (2001)
32. Emig, T., Hanke, A., Golestanian, R., Kardar, M.: Normal and lateral Casimir forces between deformed plates. *Phys. Rev. A* **67**, 022114 (2003)
33. Emig, T., Jaffe, R.L., Kardar, M., Scardicchio, A.: Casimir interaction between a Plate and a Cylinder. *Phys. Rev. Lett.* **96**, 080403 (2006)
34. Feinberg, G., Sucher, J.: General Form of the Retarded van der Waals Potential. *J. Chem. Phys.* **48**, 3333–3334 (1968)
35. Feinberg, G., Sucher, J.: General Theory of the van der Waals interaction: A Model-Independent Approach. *Phys. Rev. A* **2**, 2395–2415 (1970)
36. Feynman, R.P., Hibbs, A.R.: *Quantum Mechanics and Path Integrals*. McGraw-Hill, New York (1965)
37. Geim, A.: Everyone's Magnetism. *Phys. Today* **51(9)**, 36–39 (1998)
38. Genet, C., Lambrecht, A., Reynaud, S.: Casimir force and the quantum theory of lossy optical cavities. *Phys. Rev. A* **67**, 043811 (2003)
39. Gies, H., Klingmüller, K.: Casimir Edge Effects. *Phys. Rev. Lett.* **97**, 220405 (2006)
40. Golestanian, R.: Casimir-Lifshitz interaction between dielectrics of arbitrary geometry: A dielectric contrast perturbation theory. *Phys. Rev. A* **80**, 012519 (2009)
41. Golestanian, R., Kardar, M.: Mechanical Response of Vacuum. *Phys. Rev. Lett.* **78**, 3421–3425 (1997)
42. Golestanian, R., Kardar, M.: Path-integral approach to the dynamic Casimir effect with fluctuating boundaries. *Phys. Rev. A* **58**, 1713–1722 (1998)
43. Graham, N., Jaffe, R.L., Khemani, V., Quandt, M., Scandurra, M., Weigel, H.: Casimir energies in light of quantum field theory. *Phys. Lett. B* **572**, 196–201 (2003)
44. Graham, N., Quandt, M., Weigel, H.: *Spectral Methods in Quantum Field Theory*. Springer-Verlag, Berlin (2009)
45. Graham, N., Shpunt, A., Emig, T., Rahi, S.J., Jaffe, R.L., Kardar, M.: Casimir force at a knife's edge. *Phys. Rev. D* **81**, 061701(R) (2010)
46. Harber, D.M., Obrecht, J.M., McGuirk, J.M., Cornell, E.A.: Measurement of the Casimir-Polder force through center-of-mass oscillations of a bose-einstein condensate. *Phys. Rev. A* **72**, 033610 (2005)
47. Henseler, M., Wirzba, A., Guhr, T.: Quantization of HyperbolicN-Sphere Scattering Systems in Three Dimensions. *Ann. Phys., NY* **258**, 286–319 (1997)
48. Jaekel, M.T., Reynaud, S.: Casimir force between partially transmitting mirrors. *J. Physique I* **1**, 1395–1409 (1991)
49. Jones, T.B.: *Electromechanics of Particles*. Cambridge University Press, Cambridge (1995)
50. Kats, E.I.: Influence of nonlocality effects on van der Waals interaction. *Sov. Phys. JETP* **46**, 109 (1977)
51. Kenneth, O., Klich, I.: Opposites Attract: A Theorem about the Casimir Force. *Phys. Rev. Lett.* **97**, 160401 (2006)
52. Kenneth, O., Klich, I.: Casimir forces in a T-operator approach. *Phys. Rev. B* **78**, 014103 (2008)
53. Kim, W.J., Brown-Hayes, M., Dalvit, D.A.R., Brownell, J.H., Onofrio, R.: Anomalies in electrostatic calibrations for the measurement of the Casimir force in a sphere-plane geometry. *Phys. Rev. A* **78**, 020101(R) (2008)
54. Klimchitskaya, G.L., Mohideen, U., Mostepanenko, V.M.: The Casimir force between real materials: Experiment and theory. *Rev. Mod. Phys.* **81**, 1827–1885 (2009)
55. Krause, D.E., Decca, R.S., López, D., Fischbach, E.: Experimental Investigation of the Casimir Force beyond the Proximity-Force Approximation. *Phys. Rev. Lett.* **98**, 050403 (2007)
56. Krein, M.G.: On the trace formula in perturbation theory. *Mat. Sborn. (NS)* **33**, 597–626 (1953)
57. Krein, M.G.: Perturbation determinants and a formula for the trace of unitary and selfadjoint operators. *Sov. Math.-Dokl.* **3**, 707–710 (1962)

58. Lambrecht, A., Neto, P.A.M., Reynaud, S.: The casimir effect within scattering theory. *New J. Phys.* **8**, 243 (2006)
59. Lamoreaux, S.K.: Demonstration of the Casimir Force in the 0.6 to $6\mu\text{m}$ Range. *Phys. Rev. Lett.* **78**, 5–8 (1997)
60. Landau, L.D., Lifshitz, E.M.: *Electrodynamics of continuous media*. Pergamon Press, Oxford (1984)
61. Levin, M., McCauley, A.P., Rodriguez, A.W., Reid, M.T.H., Johnson, S.G.: Casimir repulsion between metallic objects in vacuum. [arXiv:1003.3487](https://arxiv.org/abs/1003.3487) (2010)
62. Li, H., Kardar, M.: Fluctuation-induced forces between rough surfaces. *Phys. Rev. Lett.* **67**, 3275–3278 (1991)
63. Li, H., Kardar, M.: Fluctuation-induced forces between manifolds immersed in correlated fluids. *Phys. Rev. A* **46**, 6490–6500 (1992)
64. Lifshitz, E.M.: *The Theory of Molecular Attractive Forces between Solids*. *Sov. Phys. JETP* **2**, 73–83 (1956)
65. Lifshitz, E.M., Pitaevskii, L.P.: *Statistical Physics Part 2*. Pergamon Press (1980)
66. Lippmann, B.A., Schwinger, J.: Variational principles for scattering processes. i. *Phys. Rev.* **79**, 469–480 (1950)
67. Milton, K.A., Parashar, P., Wagner, J.: Exact results for Casimir interactions between dielectric bodies: The weak-coupling or van der waals limit. *Phys. Rev. Lett.* **101**, 160402 (2008)
68. Milton, K.A., Parashar, P., Wagner, J.: From multiple scattering to van der waals interactions: exact results for eccentric cylinders. [arXiv:0811.0128](https://arxiv.org/abs/0811.0128) (2008)
69. Mohideen, U., Roy, A.: Precision Measurement of the Casimir force from 0.1 to $0.9\mu\text{m}$. *Phys. Rev. Lett.* **81**, 4549–4552 (1998)
70. Morse, P.M., Feshbach, H.: *Methods of Theoretical Physics*. McGraw-Hill, New York (1953)
71. Munday, J.N., Capasso, F.: Precision measurement of the Casimir-Lifshitz force in a fluid. *Phys. Rev. A* **75**, 060102(R) (2007)
72. Munday, J.N., Capasso, F., Parsegian, V.A.: Measured long-range repulsive Casimir-Lifshitz forces. *Nature* **457**, 170–173 (2009)
73. Palasantzas, G., van Zwol, P.J., De Hosson, J.T.M.: Transition from Casimir to van der Waals force between macroscopic bodies. *Appl. Phys. Lett.* **93**, 121912 (2008)
74. Parsegian, V.A.: *van der Waals Forces*. Cambridge University Press, Cambridge (2005)
75. Rahi, S.J., Emig, T., Graham, N., Jaffe, R.L., Kardar, M.: Scattering theory approach to electrodynamic Casimir forces. *Phys. Rev. D* **80**, 085021 (2009)
76. Rahi, S.J., Emig, T., Jaffe, R.L., Kardar, M.: Casimir forces between cylinders and plates. *Phys. Rev. A* **78**, 012104 (2008)
77. Rahi, S.J., Kardar, M., Emig, T.: Constraints on stable equilibria with fluctuation-induced forces. [arXiv:0911.5364](https://arxiv.org/abs/0911.5364) (2009)
78. Rahi, S.J., Rodriguez, A.W., Emig, T., Jaffe, R.L., Johnson, S.G., Kardar, M.: Nonmonotonic effects of parallel sidewalls on Casimir forces between cylinders. *Phys. Rev. A* **77**, 030101(R) (2008)
79. Rahi, S.J., Zaheer, S.: Stable Levitation and Alignment of Compact Objects by Casimir Spring Forces. *Phys. Rev. Lett.* **104**, 070405 (2010)
80. Reid, M.T.H., Rodriguez, A.W., White, J., Johnson, S.G.: Efficient Computation of Casimir Interactions between Arbitrary 3D Objects. *Phys. Rev. Lett.* **103**, 040401 (2009)
81. Renne, M.J.: Microscopic theory of retarded Van der Waals forces between macroscopic dielectric bodies. *Physica* **56**, 125–137 (1971)
82. Robaschik, D., Scharnhorst, K., Wierzchorek, E.: Radiative corrections to the Casimir pressure under the influence of temperature and external fields. *Ann. Phys., NY* **174**, 401–429 (1987)
83. Rodriguez, A., Ibanescu, M., Iannuzzi, D., Capasso, F., Joannopoulos, J.D., Johnson, S.G.: Computation and visualization of Casimir forces in arbitrary geometries: Non-monotonic lateral-wall forces and failure of proximity force approximations. *Phys. Rev. Lett.* **99**, 080401 (2007)
84. Rodriguez, A.W., Joannopoulos, J.D., Johnson, S.G.: Repulsive, nonmonotonic Casimir forces in a glide-symmetric geometry. *Phys. Rev. A* **77**, 062107 (2008)

85. Rodriguez-Lopez, P., Rahi, S.J., Emig, T.: Three-body Casimir effects and nonmonotonic forces. *Phys. Rev. A* **80**, 022519 (2009)
86. Rosa, F.S.S.: On the possibility of Casimir repulsion using Metamaterials. *J. Phys.: Conf. Ser.* **161**, 012039 (2009)
87. Rosa, F.S.S., Dalvit, D.A.R., Milonni, P.W.: Casimir-Lifshitz Theory and Metamaterials. *Phys. Rev. Lett.* **100**, 183602 (2008)
88. Roy, A., Lin, C.Y., Mohideen, U.: Improved precision measurement of the Casimir force. *Phys. Rev. D* **60**, 111101(R) (1999)
89. Schaden, M., Spruch, L.: Infinity-free semiclassical evaluation of Casimir effects. *Phys. Rev. A* **58**, 935–953 (1998)
90. Schwinger, J.: Casimir effect in source theory. *Lett. Math. Phys.* **1**, 43–47 (1975)
91. Tira, C.C., Fosco, C.D., Losada, E.L.: Non-superposition effects in the Dirichlet Casimir effect. *J. Phys. A: Math. Theor.* **43**, 235402 (2010)
92. Weber, A., Gies, H.: Interplay between geometry and temperature for inclined Casimir plates. *Phys. Rev. D* **80**, 065033 (2009)
93. Wirzba, A.: Quantum mechanics and semiclassics of hyperbolic n-disk scattering systems. *Phys. Rep.* **309**, 1–116 (1999)
94. Wirzba, A.: The Casimir effect as a scattering problem. *J. Phys. A: Math. Theor.* **41**, 164003 (2008)
95. Zaheer, S., Rahi, S.J., Emig, T., Jaffe, R.L.: Casimir interactions of an object inside a spherical metal shell. *Phys. Rev. A* **81**, 030502(R) (2010)
96. Zhao, R., Zhou, J., Koschny, T., Economou, E.N., Soukoulis, C.M.: Repulsive Casimir Force in chiral metamaterials. *Phys. Rev. Lett.* **103**, 103602 (2009)